NASA TECHNICAL NOTE

NASA TN D-6665

MEASURED PERFORMANCE OF A 1089 K (1500° F) HEAT STORAGE DEVICE FOR SUN-SHADE ORBITAL MISSIONS

by David Namkoong

Lewis Research Center
Cleveland, Ohio 44135

NATIONAL AERONAUTICS AND SPACE ADMINISTRATION • WASHINGTON, D. C. • FEBRUARY 1972

1. Report No. NASA TN D-6665	2. Government Accession No.	3. Recipient's Catalog No.
4. Title and Subtitle MEASURED PERFORMANCE OF A 1089 K (1500° F) HEAT STORAGE DEVICE FOR SUN-SHADE ORBITAL MISSIONS		5. Report Date February 1972 6. Performing Organization Code
7. Author(s) David Namkoong		8. Performing Organization Report No. E-6511 10. Work Unit No. 112-27
9. Performing Organization Name and Address Lewis Research Center National Aeronautics and Space Administration Cleveland, Ohio 44135		11. Contract or Grant No. 13. Type of Report and Period Covered Technical Note
12. Sponsoring Agency Name and Address National Aeronautics and Space Administration Washington, D.C. 20546		14. Sponsoring Agency Code

15. Supplementary Notes

16. Abstract

Tubes designed for a solar heat receiver to serve as an energy source for a Brayton power system were tested for 2002 hours and 1251 sun-shade cycles. The tubes were designed to transfer a constant thermal input to the Brayton system during an orbit. Excess solar energy during a sun period is stored as heat of fusion of lithium fluoride. The niobium - 1-percent zirconium tubes accommodate the 23 percent volume decrease of LiF during freezing. Test results showed slight, local distortions. The gas discharge temperature varied from 16 K (29° F) below to 28 K (50° F) above the nominal value of 1089 K (1500° F). The tube surface temperatures ranged from 1039 K (1410° F) to 1183 K (1670° F).

17. Key Words (Suggested by Author(s))	18. Distribution Statement
Heat storage Solar receiver Brayton cycle Lithium fluoride tubes	Unclassified - unlimited

19. Security Classif. (of this report)	20. Security Classif. (of this page)	21. No. of Pages	22. Price*
Unclassified	Unclassified	00	$3.00

* For sale by the National Technical Information Service, Springfield, Virginia 22151

MEASURED PERFORMANCE OF A 1089 K (1500° F) HEAT STORAGE DEVICE FOR SUN-SHADE ORBITAL MISSIONS

by David Namkoong

Lewis Research Center

SUMMARY

The effective use of a space power system based on the Brayton cycle with solar heating is highly dependent on the performance of the solar-heat receiver. This receiver must store excess solar energy during the sunlit period and then transfer this stored energy to the Brayton system during shade time in order to maintain constant thermal input over the entire orbit. In the receiver design, the heat storage and heat transfer to the Brayton cycle working fluid (gas) is accomplished by the use of coaxial tubes. The gas flows through the inner tube; the heat storage medium, lithium fluoride (LiF), is located in the annulus; and the incoming heat is transmitted through the outer tube. The tubes were designed to operate under gravity conditions ranging from 0 to 1 g. The outer (coaxial) tube is convoluted so that the LiF would remain distributed along the flow length in nearly self-contained units. Both tubes are made of niobium - 1-percent zirconium.

As part of the development of the full receiver, tests were conducted on three receiver tubes under conditions simulating a near Earth orbital mission (except for gravity); that is, within a vacuum chamber and with radiant heaters on a 60-minutes-on, 36-minutes-off continuous cycle. The initial test was conducted with a high-solar-absorptance coating, iron titanate, on the outside surface of the convoluted tube. After 150 hours of testing, the coating was found to have decomposed and the base metal to be contaminated with oxygen from the coating. In the second phase of testing, no coating was used; instead, the bare niobium - 1-percent zirconium tube surface was grit-blasted to increase its solar absorptance. Results showed that the grit-blasted approach provided a stable surface with adequate solar absorptance.

Testing proceeded for 2002 hours with 1251 sun-shade cycles before terminating in a scheduled shutdown. Post-test inspection revealed no gross distortions, but local distortions did occur in individual convolutions in the gas-inlet region. Measured temperatures along the tube ranged from 1039 to 1183 K (1410° to 1670° F). In addition, the temperature at each tube-surface location varied during a typical sun-shade cycle. This variation in tube temperature was at least partly reflected in the gas-discharge temperature. The gas varied from 16 K (29° F) below to 28 K (50° F) above the nominal value of 1089 K (1500° F) and was repeatable for the 1251 cycles. This variation is within the design goal of receiver performance.

INTRODUCTION

In space, electric power can be generated by the conversion of solar heat. If a solar-heated powerplant is in Earth orbit, however, there will be portions of the orbit during which the powerplant is in the Earth's shadow. A design of such a powerplant in an orbiting craft should therefore consider the storage of thermal energy for use during the shadow period. One system that could be considered for an orbital mission and that could utilize solar energy is based on the Brayton cycle. The Brayton cycle configuration (fig. 1), employs a dynamic power system in which the working fluid receives energy from the sun and converts it to electrical energy through the turbomachinery.

At the present time a Brayton-cycle system is being investigated at the Lewis Research Center primarily for use with an isotope heat source. From cycle and thermal property considerations the working fluid chosen is a mixture of helium and xenon gases having the molecular weight of krypton. This same system could be used with solar heating as well. To provide for this solar-heating option, a solar heat-receiver has been designed and fabricated. A photograph of the actual 48-tube, solar-heat receiver is shown in figure 2.

In the receiver design heat storage and the heat transfer to the helium-xenon gas are accomplished by the use of the coaxial tubes. Gas flows through the inner tube, and the heat-storage medium (lithium fluoride) is confined within the annular volume (fig. 3). The varying distribution of lithium fluoride (LiF) along the axial length, and therefore the tapering volume distribution of the convoluted tube are the results of the required heat-flux distribution. The choice of LiF was made on the basis of its adequate heat of fusion at the temperature level required by the cycle. During the sunlit period of the orbit, part of the heat transferred through the outer-tube surface is transferred to the flowing gas. The remaining heat liquifies the LiF. During the shadow period, the liquid LiF solidifies, giving up its latent heat to the gas. In this way the gas-discharge temperature is expected to stay essentially constant during the entire orbit.

A prime concern in the design of the tubes was that of controlling the distribution of the LiF. In changing from a liquid to a solid phase, the LiF undergoes a 23-percent decrease in volume. Without due consideration for this shrinkage, the void volume could be distributed adversely and cause varying heating of the gas. Without LiF in contact with the tube surface in order to absorb some of the solar energy incident on that region, the outer-tube surface could overheat during the sunlit period. The requirement that the tubes must be able to operate under 1-g as well as 0-g conditions further aggravates the LiF-distribution problem.

The design on which the tubes were built calls for a convoluted outer tube, the diameter of the neck of which is within 0.76 millimeter (0.030 in.) of the inner tube. At the onset of freezing, the minimum clearance between the tubes is expected to be plugged

with solid LiF, sealing the remaining LiF within each convolution. In this way LiF would remain properly distributed along the active heat-transfer length of the tube during melting and freezing, under either 1 or 0 g.

The inner tube is 3.18 centimeters (1.25 in.) in diameter with circumferential grooves rolled at 2.5-centimeter (1-in.) intervals. The grooves serve to increase the gas-side convective heat-transfer coefficient to that value required to attain the design discharge temperature. An independent test was conducted to determine the groove depth required. The procedure is described in the appendix.

Niobium - 1-percent zirconium (Nb-1Zr) was used for the tube material as well as being used throughout the heat receiver. The high conductivity, the low elastic modulus, the low coefficient of thermal expansion, and the temperature tolerance of this refractory metal allow latitude in designing for extended structural life at the expected elevated temperature levels.

The heat-flux distribution absorbed by the convoluted tube depends on the absorptive and emissive properties of the surface. Since the gas-side capability was designed on the basis of a heat flux distribution close to that of the incident solar flux, a high value of solar absorptance was deemed necessary. An analysis described in reference 1, confirms the importance of surface absorptance within the receiver. To obtain a high value of solar absorptance, the tubes were coated with iron titanate. To obtain a high value without a coating, another set of tubes was grit blasted. Both types of surfaces were tested.

In this investigation, the heat-storage tube design was evaluated in terms of its impact on the performance of the total receiver. As such, the following items were deemed as key areas of concern:

(1) Heat transfer to the gas

(2) Pressure drop of the gas

(3) Variation in gas outlet temperature during the orbital period

(4) Localization of the LiF (Do the convolutions adequately prevent longitudinal migration of the LiF, or is the migration so serious that thermal performance is impaired?)

(5) Mechanical integrity of the tubes (Do the convolutions distort or fail in fatigue under the thermal cycling imposed by successions of sun-shade operation?)

(6) Stability of iron titanate in this application.

A complete thermal analysis of the solar-receiver tubes that adequately evaluates its performance is a formidable task. Any analysis or experimental investigation that has been undertaken thus far on a heat-storage design has been based on relatively simple geometries, most noteworthy being those mentioned in references 2 to 4. The configurations studied included the heat-storage medium (LiF or LiH) between two thick plates with and without fins, and also included tubes containing flowing gas, immersed in the medium.

The present design, consisting of a convoluted geometry, renders a difficult heat-transfer analysis. This is apparent when one considers such factors within a single convolution as the continually varying phase percentage of the LiF during the sun-shade cycle, void formation and distribution as the LiF solidifies, nonuniform circumferential heating, and thermal radiation between the given convolution and the total receiver. These factors all affect the heat transfer from a convolution to the gas and, cumulatively, affect the gas-discharge temperature. These factors also determine the thermal stresses on the convolutions.

Because of the complexity of the analysis, it was decided to evaluate the receiver tube design experimentally by subjecting three such tubes to conditions simulating an orbital mission. A configuration of three tubes, side by side, was chosen with the two outside tubes used as guards to provide the correct thermal environment for the center tube. In this way the middle tube would experience the same radiation interchange with the adjacent tubes as in the receiver. The tubes were tested in a vacuum chamber and exposed to zoned electric heaters, axially distributed to simulate the solar heat flux. In simulation of a low-altitude orbit, the heat-input rate was applied periodically, 60 minutes on and 36 minutes off. Test time under these simulated conditions totaled 2002 hours. Helium-xenon was circulated through the tubes under conditions simulating operation in the Brayton power system. Surface temperatures on the tubes, gas temperatures entering and leaving the tubes, and pressure drop through the tubes were measured.

This report evaluates the heat-storage tube design by presenting the performance and post-test examination of the 2002-hour test of these three tubes.

APPARATUS

Test Section

The three receiver tubes and the tantalum heaters (to simulate the distribution of solar flux to the tubes) were mounted within a water-cooled copper box. The relative position between the tubes and the heaters is shown in figure 4. The test section was designed to contain the tubes within one-half of the copper box (fig. 5) and the heaters within the mating half (fig. 6). Niobium and molybdenum sheets functioned as radiation shields between the interior and the wall of the copper box.

The three Nb-1Zr receiver tubes are of identical design: a 37-convolution tube fitted coaxially over a 3.18-centimeter (1.25-in.) diameter tube. The convolution tube is made up of disks formed into half convolution shapes and electron-beam welded together.

Dimensions are indicated in figure 7 and in tables I to III. The volume between the tubes was filled with molten LiF at a fill temperature of 1228 K (1750° F). This temperature is 106 K (190° F) above the LiF's melting temperature. It is also about 50 K (90° F) above the hottest temperature at which the receiver is expected to operate, thus providing additional volume for thermal expansion. Two 3.2-millimeter (0.125-in.) diameter tubes, one welded to each end convolution, were used to fill the entire tube with LiF. A radial clearance of 0.4 millimeter (0.015 in.) is provided between the neck of the convolutions and the inside tube to allow for transfer of the molten LiF from one convolution to the next during the filling operation. This small annulus, as mentioned previously, enables a frozen LiF barrier to be formed readily during an orbital mission thereby maintaining the proper distribution of LiF along the tube. The inside tube through which the gas flows is grooved circumferentially every 2.5 centimeter (1 in.) for 92 centimeters (36 in.).

In the initial performance tests, the outer surface of the convolutions was coated with plasma-sprayed iron titanate (Fe_2TiO_5). For the endurance test, no coating was used. Instead, the outer surface was grit-blasted with 406-micrometer aluminum oxide particles. The abrasive shape was intermediate between being blocky with sharp edges and being slivery with very sharp edges. In both the coating and grit-blasted cases the intent was to produce a high solar-absorptive, emissive surface. Reference 1 discusses the influence of a range of these radiation properties and concludes that while both are important to receiver performance, solar absorptance is primarily so. Though the iron titanate coating indicated higher absorptance values and therefore was more desirable, there was a chemical breakdown of the coating during the initial test. This result precipitated the decision to switch to the grit-blasted tubes. The coating breakdown is described in detail in a later section of this report.

Heaters within the test section fall into two classifications - the primary heater, which basically provides the distribution of the solar heat flux, and the guard heater, which is used to eliminate heat loss from the back side of the primary heater. Two radiation shields separate the primary heater from the guard. The primary heater is divided into 15 zones ranging in length from 5 to 10 centimeters (2 to 4 in.) along the tube axis. The guard heater is divided into four zones ranging from 20 to 30 centimeters (8 to 12 in.) along the axial length. Each zone in both the primary and guard heaters is separately controlled.

Radiation shielding in the form of four thin sheets (innermost sheet Nb, the outer three, Mo) was installed on all interior surfaces of the copper box except for the area behind the tubes. Here, 20 thin niobium sheets, held apart by surface dimples were installed for the initial test. For the endurance phase of testing, a 60-layer, compact, multifoil heat shield (20 layers Mo, 40 layers Ni) was added behind the tubes. The additional insulation served to reduce heat loss further.

Test Facilities

The facility used for testing the three receiver tubes featured a vacuum chamber that housed the test section and maintained pressure in the 10^{-8} torr range. The vacuum chamber is a cylindrical, stainless steel structure, with a 183-centimeter (72-in.) inside diameter and a 1.8-centimeter (0.500-in.) wall, oriented with its axis vertical for an overall height of 345 centimeters (136 in.). Vacuum is attained in two stages: by roughing holding pumps, which reduce the vacuum tank pressure from atmospheric to the 10^{-4} torr range and by oil diffusion pumps, which reduce the pressure further. Three 25-centimeter (10-in.) oil diffusion pumps were used in the test. Heater power of 5400 watts was used for each pump. Liquid nitrogen was also used for a baffled cold wall inside the chamber. The cold wall is a cylindrical copper shell, with a 1.7-meter (5.5-ft) outside diameter and 1.5 meters (5 ft) high, and is used to adsorb gas molecules onto its surface. Using this system, vacuum levels of 10^{-8} torr were readily maintained.

The closed-loop gas system is shown schematically in figure 8. In operation, a diaphragm compressor was the driving force to circulate the gas around the loop. A bypass line was incorporated to control the flow rate to the test section. The discharge gas from the compressor was passed through a water-cooled heat exchanger so that its flow rate could be measured at a constant temperature. Because diaphragm compressors are known to operate with a significant amount of pressure oscillation, surge tanks were installed on both the upstream side of the compressor and the downstream side to minimize this effect. The pressure oscillations during test were damped from approximately ±7 newtons per square centimeter (10 psi) at the compressor to ±0.17 newton per square centimeter (0.25 psi) at the test section. Gas flow rate was measured before the flow was divided as well as in each of the three lines. Flow rate was controlled by a valve in each line. A finned heater rod functioning as a preheater heated the flowing gas from room temperature to approximately the design inlet temperature. A trim heater further downstream provided fine control of gas-inlet temperature to each tube. Zirconium chips within the tube section heated by the trim heater served as an oxygen and nitrogen getter for the flowing gas to prevent contamination of the niobium tubes. Originally, all three lines contained the chips, but the oxygen and nitrogen levels as read by the mass spectrometer indicated that using one line only to contain the chips was sufficient.

The gas then passed through the test section oriented so that the tubes were $21\frac{1}{2}^{\circ}$ from the vertical, the same angle as the tubes in the receiver with the receiver axis vertical. This can be seen in figure 9, a photograph taken with the lid and cold wall removed from the vacuum chamber. From the test section, the three lines merge, pass through the vacuum tank wall and into two water-cooled heat exchangers. The throttle

valve controls the pressure level within the test section. Cooled to room temperature, the gas returns to the compressor to be recirculated.

Bimetallic joints were used to provide the tube-to-tube connection between the stainless steel and the niobium. These joints were of tongue-in-groove brazed design as shown in figure 10 and used at the inlet and discharge for each of the three receiver tubes.

In addition to the basic gas loop, provisions were made to recover the working gas upon loop shutdown, to inject helium-xenon from the gas supply bottle, and to add pure helium to the loop (in the event of its preferential leakage).

INSTRUMENTATION

Temperatures on the niobium receiver tubes and backing sheet were measured by calibrated platinum/platinum - 13-percent rhodium (Pt/Pt13Rh), 24-gage thermocouples connected to two 24-channel Brown recorders. The original thermocouple calibration showed a maximum deviation of 0.8 K (1.5° F) higher than the reference reading (according to NBS Circular 561) in the temperature range of expected operations. A recalibration after test was conducted on a thermocouple that was attached to tube 2 in the high-heat flux region. With an immersion of 15.2 centimeters (6 in.) in the reference oven, the thermocouple indicated 0.4 K (0.7° F) higher and 0.8 K (1.4° F) lower than reference temperatures at 944 K (1240° F) and 1250 K (1792° F), respectively. Within the test section, all Pt/Pt13Rh thermocouples had a minimum of 15.2 centimeters (6 in.) exposed to near isothermal surroundings.

The same type of thermocouple was attached to the two shields between the primary and guard heaters and connected to indicators. Those temperatures that were not expected to exceed 370 K (200° F) (usually associated with water-cooled components) were measured by means of iron-constantan thermocouples. The remaining thermocouples were Chromel-Alumel. Both the iron-constantan and Chromel-Alumel wires met the ISA specifications.

Of special interest regarding thermocouple use is the temperature measurement of the gas into and out of the receiver tubes. To measure the bulk gas temperature, each thermocouple was incorporated into a flow mixer. The mixer was designed to force the gas to flow turbulently in continually changing directions so that the thermocouples would be measuring a true averaged gas temperature. Initially, the flow mixer was separated from the receiver tube by a 90° elbow and a Nb-1Zr/stainless steel transition joint. Tests with this original scheme indicated excessive heat loss taking place between the receiver tubes and the mixers. For the endurance test a new flow-mixing section was designed to be positioned close to the active length of the receiver tube.

This design is shown in figure 11. Because it was designed to fit inside the 3.18-centimeter (1.25-in.) tube, this section was positioned to within 2.5 centimeter (1 in.) of the last convolution of the tube. This design features both external and internal radiation shields to minimize heat loss or heat addition to the mixed gas. The gas-inlet temperature was measured in the same manner.

Helium-xenon pressures throughout the system were measured by Bourdon tube gages. Where accurate readings were required, such as at the receiver tube inlet and those needed to determine gas flow rate, the gages were accurate to 0.1 percent of full scale. Since 69-newton-per-square-centimeter (100-psi) gages were used, accuracy was within 0.7 newton per square centimeter (0.1 psi). Certified calibration indicated that the accuracy was within the specification.

Pressure drop through the receiver tube was measured only during the initial tests. Measurement was made by a visual, direct-reading diaphragm differential gage with a maximum range of 750 newtons per square meter (3 in. of water). The accuracy was ±2 percent of full scale or a maximum error of 14.9 newtons per square meters (0.06 in. of water). For the endurance test, there was no attempt to measure the receiver tube pressure drop. This was due to the placement of the relatively high-pressure-drop flow mixers within the tubes that would have completely overshadowed the receiver tube measurement.

Rotameters were used to measure helium-xenon flow rate. The instruments were calibrated by a positive displacement wet test meter that was accurate to 1 percent of the flow rate in the range of use. Air was used as the calibrating fluid at the expected density for the test condition with helium-xenon. The actual difference in density was duly accounted for.

A mass spectrometer was used to ascertain the composition of the working fluid. The mass spectrometer was connected to both the fluid in the gas loop and to the gas supply. In this way, the gas supply served as a reference with which to compare the gas in the system. The accuracy of the mass spectrometer is very much dependent on the scale of measurement, that is, whether the gas component that is measured is a major constituent or a minute contaminant of the sample. The error introduced by the electrical "noise" and drift in the spectrometer amounted to two divisions (full scale chart output = 100 divisions). The difference of the gas constituents (the contaminants as well as helium and xenon) between the loop and the gas supply was within two divisions throughout the testing period. This means that the helium and xenon molar percentages in the gas loop were 38.5±1.3 percent and 61.5±2.1 percent, respectively; and that the contaminants in the gas loop differed by less than 1 molar ppm from the reference.

EXPERIMENTAL PROCEDURE

The test of the three solar receiver tubes was originally conceived in two phases - a short-term test to evaluate performance, and an endurance test to determine any change in performance over a relatively long period of time. A comparison of the two tests is shown in the following tabulation.

Type of test	Test duration, hr	Tube surface	Basis of heat flux
Short term	131	Coated with iron titanate	Incident solar flux
Endurance	2002	Grit blasted	Incident solar flux plus receiver cavity reflections

In the first test, a coating of iron titanate (Fe_2TiO_5) was used to increase the emittance and solar absorptance of the tubes. The iron titanate was in the form of powder that was plasma-sprayed at Lewis onto the tubes, reflectors, and backing sheet. In the second test, the bare niobium surfaces of three new tubes were grit blasted by aluminum oxide particles to increase the emittance and solar absorptance. The solar flux incident on the tubes was calculated for the reflection from a 9.15-meter (30-ft) parabolic mirror and a solar half angle of $0^{o}16'$. The incident flux distribution is shown as the higher peaked curve in figure 12. The curve was obtained through use of a computer code developed by Schrenk (ref. 5). The short-term test was based on the distribution of full absorption of the incident solar flux. For the endurance test, the net input flux to the tubes was used. This flux distribution (the second curve in fig. 12) is also based on the incident solar flux but is modified by loss through the receiver aperture and the reflective interchange within the receiver cavity. The full analysis resulting in this curve is described in reference 1.

The three-tube test was designed to operate at the same condition of gas flow per tube as in a solar receiver 11-kW_e Brayton system. The cycle information is as follows:

Working fluid	He-Xe gas mixture
Molecular weight	83.8
Total flow rate through receiver, kg/sec (lb/sec)	0.726 (1.6)
Receiver gas-inlet temperature, K (^{o}F)	865 (1098)
Receiver gas-inlet temperature, K (^{o}F)	1089 (1500)
Receiver gas pressure, N/cm^{2} (psia)	36.5 (53)

Performance evaluation was based on the physical results of the test - dimensional and metallographical - and on test data such as temperature on the convoluted tube surface and on the backing sheet, the discharge gas temperature, and pressure drop.

The environmental condition that was to be simulated was that of a vacuum and a cyclic heat loading of 60 minutes sun, 36 minutes shade. This condition is equivalent to a circular near Earth orbit to approximately 1600 kilometers (1000 miles) - the plane of which includes the Sun-Earth line. In an actual orbital mission, however, the duration of shade can vary from 0 to 36 minutes, the extent of variation depends on the angle of the orbit with the ecliptic plane. A constant shade time of 36 minutes each cycle, therefore, imposes a condition of minimum integrated heat input per orbit to the receiver tubes.

The sun-shade simulation was provided by an integral unit incorporating both the timing sequence function and the power controllers. The timing was controlled by a constant-speed rotating drum. Tabs on the drum were positioned to switch the sun condition power setting or the shade condition power setting into the circuit at the appropriate time. Power to the heater was necessary for the shade condition to compensate for the greater heat losses in the test section compared to actual receiver conditions. In the first test, there was one bank of power controllers with which to control the two settings (sun and shade). As a result, the power had to be reset manually at every switchover. In the second test, a second bank of controllers was added. With one bank set for the sun condition and the other set for the shade, the operation became entirely automatic.

The condition for startup included the pressurization of the gas loop to approximately 48 newtons per square centimeters (70 psia) with helium, and the vacuum level within the vacuum chamber in the low 10^{-7} torr range. Startup was initiated by applying power to the primary and guard heaters of the test section. The rate of average temperature rise of the receiver tubes was controlled to stay within the following limits:

At 533 K (500^{o} F) pressure no greater than 5×10^{-5} torr

At 811 K (1000^{o} F) pressure no greater than 1×10^{-6} torr

At 1089 K (1500^{o} F) pressure no greater than 5×10^{-7} torr.

The limits were based on information from reference 6. Liquid-nitrogen flow through the cold wall within the tank helped maintain the vacuum levels.

The heat loss distribution from the test section at a uniform tube-surface temperature was determined by ascertaining the difference between the power distributions for the flow and no-flow conditions. Receiver tube flow was established at its design rate, and its design inlet temperature. Uniform tube temperatures at 867, 1006, 1102, and 1144 K (1100^{o}, 1350^{o}, 1525^{o}, and 1600^{o} F) ensured that heat losses would be measured over the full range of operations.

RESULTS AND DISCUSSION

Short-Term Test

Within a short period of time after starting, a trend toward higher tube temperature at the end of each succeeding cycle was noticed. When the maximum temperature of 1228 K (1750^{o} F) was reached, the flux was reduced by 10 percent and was maintained at this value for the remainder of the test. The pressure drop between the inlet and the discharge was 249 newtons per square meter (1 in. of water). The reading did not change with the sun and shade periods during a cycle.

The test continued for 131 hours and 82 cycles before concluding in a scheduled shutdown. The test section was removed from the gas loop and photographed. The tubes were then separated from the test section and sectioned to ascertain LiF distribution. The iron titanate coating was metallographically analyzed.

When the test section was opened, the tubes appeared to be in good condition physically (fig. 13); there were no apparent distortions of any convolution and no bowing of the tubes. There were, however, whitish zones on the convolutions resembling water stains (fig. 14). Consequently, four samples of the coating were taken for an X-ray diffraction analysis. The samples were taken from the whitish zones of the first, 20th, and 30th convolutions of the center tube and from an apparently unaffected zone of a convolution of a flanking tube. The results showed that the iron titanate (Fe_2TiO_5) had decomposed and that the samples from the whitish zones showed the greatest effect. In these areas, there were strong indications of αFe (free iron) and TiO_2. The sample from the flanking tube showed strong $FeTiO_3$ and TiO_2 with a medium indication of Fe_2TiO_5. These findings correspond with those of Harrison and Hendrixson of the General Electric Co. (under NASA Contract NAS 3-8523), which also showed the whitish zones. Their analyses included picturing the iron in the coating, after test, in large discrete nodules in contrast to the uniform distribution of iron and titanium before test. The breakdown included a release of the oxygen to be absorbed by the niobium alloy substrate. Contamination levels of Harrison and Hendrixson reached into the 2000 ppm range after 3000 hours of testing.

The center tube was sectioned lengthwise to ascertain the LiF distribution in each convolution as well as along the length of the tube. Figures 15 and 16 show the views inside the convolutions on the heater side and toward the opposite side, respectively. The LiF is shown to have frozen mostly on the side that was heated which is also that side favored by gravity. The five exit-end convolutions are shown to be virtually empty of any LiF. Since the LiF was loaded at 1228 K (1750^{o} F), some of the void volume is attributable to the contraction of the liquid from 1228 K (1750^{o} F) to its freezing temperature of 1122 K (1560^{o} F). This was calculated to be equivalent to approximately $2\frac{1}{2}$ convolutions in the discharge region. The other influence is the effect of gravity in draining off that volume of liquid and distributing it to the convolutions below. The very bottom (inlet region) convolutions appear to include more frozen LiF than some others of equal capacity in the same region. The short-term test indicated areas where improvements were needed to obtain accurate data. These included a closer coupling of the gas temperature sensors to the convoluted tubes and an automated system to switch from power settings of sun to shade. These features were incorporated for the endurance test.

Endurance Test Results

The endurance test imposed essentially the same conditions on the second set of tubes (consisting of grit-blasted bare Nb-1Zr tubes) as on the first set. The imposed heat flux again had to be reduced when the maximum convolution temperature approached 1228 K (1750^{o} F). The reduction was 5 percent of the corrected incident heat flux. The endurance test consisted of 1251 sun-shade cycles and 2002 hours. Shutdown occurred as scheduled.

On completion of the endurance test, the test section was removed from the gas loop and photographed. The tubes were radiographed and dimensionally measured. The center tube was subsequently sectioned for metallographic analysis.

Physical features. - The appearance of the tubes when the test section was opened gave the general impression that it had preserved its basic physical integrity (fig. 17). There were no gross distortions of any convolution nor was there an obvious bowing of the tube axis with respect to each other. The surfaces appeared to be free of cracks and no LiF buildup was apparent to suggest LiF leak. There was, however, a blackish deposit on the tubes and on the sheet behind the tubes. The deposit (soot-like particles) was heavier toward the inlet end of the tube and virtually nonexistent toward the discharge end. The particles were easily scraped off the tube surface with parchment paper and were subsequently analyzed. The analysis will be described in more detail in the section "Metallographic Analysis."

The three tubes were radiographed to determine LiF distribution in the convolutions. Figures 18 to 20 show the three tubes at the inlet region, midregion, and exit region, respectively. The tubes are in the same relative position to each other as during the test except that each tube has been rotated 90°. The view shown, therefore, is essentially that of the tube cross section from the heater (180°) side to the backing sheet (0°) side.

In general, the intent of the convolution design, as evidenced by these radiographs, appears to have been successful in maintaining LiF along the length of the gas-flowing tube. It is evident, however, that there had been some shift in LiF distribution. The inlet region convolutions appeared to be relatively fuller than the midsection convolutions; and the discharge end region had virtually no LiF in its last several convolutions. Figure 21 shows the first (inlet) convolution of tube number 2 with its top half cut away revealing the solidified LiF. The fullness of the LiF within the convolution corroborates the indication of the radiographs. In addition, the first few convolutions in the inlet region (as seen more clearly in fig. 22) appear to be distorted. The heater side of the convolutions appears to have "swelled."

The radiographs in the middle section of the convoluted tubes (fig. 19) indicate what had been expected for the entire convoluted tube length. The amount of LiF in each of the convolutions appears to be the same as before the test. The location of the LiF indicates the influence of gravity on distribution within each convolution.

Figure 23 offers the contrast of the LiF taken from convolution number 4 near the tube inlet compared with the LiF taken from convolution number 18, in the midlength region of the center tube. The LiF from convolution number 4 appears to be an accumulation of discrete lumps that has taken several sun-shade periods to build up. The LiF from convolution number 18, on the other hand, is a clear crystalline structure that suggests total LiF melting and freezing during each orbital period.

The radiographs of the convoluted tubes at the exit section all show virtually no LiF in the last seven or so convolutions. As described in the short-term test discussion, the volume of $2\frac{1}{2}$ convolutions can be attributed to the differential contraction between the fill temperature of 1228 K (1750° F) and the freeze temperature of 1122 K (1560° F). In addition, the volume equivalent of $4\frac{1}{2}$ convolutions also must have flowed to the convolutions below. This does not mean, however, that these $4\frac{1}{2}$ convolutions necessarily remain empty during an entire orbital period. It is possible during the heating period that liquid LiF expands partially into these convolutions from the convolutions below. It does mean that even if this occurs, the LiF drains into the lower convolutions by the end of the shade period.

The changes in dimension after the test are tabulated in tables IV to VI. The change is defined as the measurement after test minus the measurement before test. The positive sign, therefore, indicates a dimensional increase as a result of the test. Dimen-

sion D was measured at the 90° and 270° planes before test and at 0°, 90°, 180°, and 270° planes after test. The change in dimension $\Delta D'$ at the 0° and 180° planes was defined as the measurement after test minus the average of the measurements at 90° and 270° before test.

Examining tables IV to VI shows that the convolution distortion in the inlet region, described qualitatively previously, can be seen in terms of dimensional changes in the ΔD and $\Delta D'$ planes. The center tube shows the distortion covering more of the convolutions than the outer tubes. This result can be expected as the two flanking tubes are fulfilling their function as a thermal barrier for the center tube and are expected to be operating cooler than the center tube. The greatest change is in the 180° plane (toward the heater) and extends from the first to the 17th convolution.

The distortion of the D dimension had the effect of drawing in the major diameter of the convolution. This can be seen by the negative signs of ΔA in those instances where ΔD and $\Delta D'$ were notably high.

The method of measurement involved in tables I to VI indicates that caution is in order when determining the significance of some of the values. No inscriptions of any kind were allowed on the tube material for measurement purposes. The intent of this prohibition was to avoid inducing a crack or other deleterious effects in the convolutions. As a result, there are rough spots that would influence diameter readings. In addition, the D dimension, the distance across the flats of a convolution, becomes almost meaningless when the contour becomes a continuously angle-changing curve. Therefore, the ΔD readings in the last few exit-end convolutions have been omitted.

Another measurement made was that of camber - the displacement of the tube axis from its true centerline at various stations along the tube length. This measurement was made with V-blocks providing end supports for the tube end with a dial indicator. With the indicator held fixed and its measuring spindle spring loaded against a convolution, the tube would be rotated 360°. The minimum and maximum readings would be noted and the circumferential angles where they occurred. The maximum displacement among the three tubes was in tube number 2. Again, this is very likely due to the higher heat input to the center tube. The maximum radial displacement measured 0.746 centimeter (0.294 in.) at the 18th and 19th convolutions. The plane of maximum displacement appeared to be slightly off 180° (more like 190°), sagging toward the heater.

Convolution temperature. - Thermocouples were attached to the convoluted tubes at five locations along the length of the tube as shown in figure 4. At each location on the center tube, four thermocouples were attached to the outer diameter, or peak, of one convolution: at the 0°, 90°, 180°, and 270° planes (refer to fig. 24 for tube orientation). In addition, a thermocouple was attached at the (upper) neck of the convolution on the 180° plane. On the flanking tubes, thermocouples were attached at the convolution peak on the 180° plane at each location. These thermocouples were intended to confirm the

readings on the center tube. The convolutions that were instrumented were numbers 3, 9, 19, 28, and 35.

Figures 25 to 29 present the variation of temperature at each location on the center tube during cycles 31, 728, and 1240. These cycles are typical of the cycles at the beginning, middle, and end of the endurance test period. The pattern in the third convolution (fig. 25) indicates that the temperature at the 180° peak position was in the molten LiF temperature range for most of the sun period and was distinctly higher than the temperature in the other positions. The temperature in the 90° peak position, in contrast, remained entirely in the solid LiF temperature range. The thermocouple at the 0° peak position became inoperative early in testing but undoubtedly would have been indicating the coldest temperatures. A significant reading is the temperature at the 180° neck position during the 1240 cycle (fig. 25(c)). The temperature increased to above 1122 K (1560° F) and presumably melted the LiF. A passage of molten LiF would have allowed accessible liquid LiF in the convolution above to have flowed into the voids of convolution number 3. The reason for the subsequent temperature drop while still in the sun period is not entirely understood. The reading was considered valid, however, since the 28th convolution also showed the same occurrence. This phenomenon is most obviously seen in figure 28(c) at the 180° neck and the 90° peak positions. Though the exact sequence of events might not be determinable, the cause of the phenomenon is easily recognized. The LiF within the convolutions was designed to function in the two-phase region; therefore, the operational condition was that of continuing change. Not only was there a constant melting and freezing of LiF, but also a change-of-phase volumetric expansion and contraction. Both of these factors contribute to a constant shifting of liquid, solid, and void volumes within each convolution. The many inflections that are common to many of the temperature curves further testify to the complex processes that took place.

Figure 26 presents the temperature variation of the ninth convolution for the 31st, 728th, and 1240th cycles. The general temperature distribution - the large difference between the temperature at the 180° peak position and the other clustered temperatures - is similar to the distribution at the third convolution. The temperature level of the ninth convolution appears to have dropped from the 31st cycle to the 728th. From the 728th cycle to the 1240th, the temperature level generally appears to have remained unchanged. The temperature variation at the 180° peak position, however, appears to have undergone a transition. Instead of a more or less constant rate of temperature rise during the sun period, the temperature during the 1240th cycle began at a lower level and suddenly rose about 22 K (40° F) over the last 20 minutes. This behavior is characteristic of a single phase response to heat input. In other words, the curve suggests that the controlling condition within the convolution, at the 180° peak position after 40 minutes, was that due to liquid LiF. The change in conditions can only be attributed to the continuously changing relation of the solid and liquid phases of the LiF and the void volume.

The temperature distribution and variation on the 19th and 28th convolutions (figs. 27 and 28) are similar. All of the temperatures appear to be responding in concert and within 14 K (25° F) of one another. All the curves show a relatively sharp increase during the sun period similar to the curve discussed for the ninth convolution. The reason for the sharp rise would be the same also - the LiF having melted entirely and further heat input resulting in the temperature rise of the LiF. As mentioned previously, there were instances of the temperature actually decreasing during the sun period such as shown in figure 28(c). It should be mentioned also that there were instances of a temperature increase during the shade period. All of the figures of the 19th and 28th convolutions include at least one curve showing this phenomenon. Again, the reason for the apparent deviation is due to the mixture of the two phases of the LiF and the void volume.

Figure 29 reflects the result of one of the exit region convolutions devoid of LiF. In this convolution (No. 35), the temperature spread is widened to as much as 39 K (70° F) - in contrast to the 14 K (25° F) spread of the previous two locations. Because of the shallow convolutions as well as the total void, there is little temperature difference between the peak and the neck at the 180° position. It may be noted that, in this region where the latent heat consideration is absent and with a constant power input to the heaters, the temperatures after the first 15 minutes in the sun period, increase at a low rate. It is evident that there is an equilibrium condition reached whereby a tendency for an increase in temperature is offset by reradiation within the test section. The equilibrium temperature under the given conditions was 1181 K (1665° F). Other locations too exhibit the temperature tapering off after an initial sharp rise. This would indicate that even with the presence of LiF the temperature of the convolution would increase after LiF melting until an equilibrium condition is reached. For the 19th and 28th convolutions the maximum equilibrium temperature was 1163 K (1633° F). Since the equilibrium temperature at a surface is heavily influenced by the other surfaces it interacts with, the equilibrium temperatures experienced in this test is expected to be different from that in the receiver.

Discharge temperature. - The working gas, helium-xenon, was maintained at a constant flow rate and inlet temperature. The discharge temperature was recorded daily throughout the endurance test. Figure 30 shows the discharge gas temperature during a full cycle at the beginning, middle, and towards the end of the test. The curves appear to exhibit the same trends as the convolution temperatures. The temperature increases relatively rapidly at the beginning of the sun period and then tends to level off. At the end of the sun period, the gas temperature drops sharply and again tends to level out. The curves themselves are not smooth but rather made up of a series of small steps and plateaus. This illustrates the result the contribution of each convolution to the total heat input to the gas.

All three curves are shown having operated on both sides of the design value of 1089 K (1500° F). The gas temperatures ranged from 16 K (29° F) below to 28 K (50° F) above the design temperature. The difference between the minimum and maximum temperatures was 36 K (65° F), 40 K (72° F), and 42 K (75° F) for the 32nd, 728th, and 1251st cycles, respectively. For the 32nd and 728th cycles the discharge temperature was above 1089 K (1500° F) for 56 minutes. For the 1251st cycle the time was 65 minutes.

Metallographic analysis. - Metallographic analysis was performed on (1) the blackish deposit on the tubes and the reflector shields and (2) the refractory material of the convolutions, reflector, shields, and the heater wire. Attention was directed on the center tube for the analyses.

The blackish deposit was obtained from the tubes and, separately, from the reflectors. The deposit was analyzed spectrographically by X-ray diffraction, and by an electron microprobe. The deposits in both cases indicate that the major constituents are niobium and aluminum. The spectrographic analysis also indicated a moderate amount of iron and titanium. This finding would indicate that iron titanate was still present despite the attempt to eliminate the coating from within the test section. The presence of aluminum raises the question as to its source. There are three possibilities - all pertaining to aluminum oxide (Al_2O_3). The first is its use as a powder that grit-blasted the surfaces exposed to the heat flux. There is a possibility that tiny particles may have become embedded in the grit-blasted surface. A second possible source is its use as insulating sleeves for the thermocouples used throughout the test section. The third possibility is its use as electrical insulators separating the tantalum heater wires from its support frame. The purity of the aluminum oxide used in the first two cases was 99.5 percent or better. A scanning electron micrograph of the deposit on a reflector section (fig. 31(a)) suggests a coral-reef type of structure. Figure 31(b) contrasts the reflector section with and without the deposit.

Analyses were also conducted on the convolution material, reflector shield, and a section of the tantalum heater wire. Material from the fourth, 18th, and the 35th convolutions (inlet, middle, discharge regions, respectively) were used as specimens. Approximate maximum temperatures at these convolutions were 1167, 1161, and 1181 K (1640°, 1630°, and 1665° F), respectively. Samples of the reflector and heater wire were taken in the high heat flux regions - approximately in the fourth convolution region. Analyses were conducted for oxygen, nitrogen, and carbon contents; the tests were performed by the inert gas fusion, Kjeldahl, and combustion chromatographic methods, respectively. All three convolutions indicated no difference in nitrogen content (71 to 82 ppm) or in carbon content (22 to 59 ppm). There was a definite gradation of oxygen content, however. The fourth convolution showed the highest reading, 2200 ppm; the 18th showed a lower value, 1200 ppm; and the 35th showed the least, 500 ppm. The original Nb-1Zr had less than 100 ppm oxygen, 50 ppm and less nitrogen, and less than

50 ppm carbon. The reflector shield sample had a reading of oxygen content that was in the same range as that of the fourth convolution. The tantalum heater wire, however, had an oxygen reading of 125 ppm, a nitrogen reading of 8 ppm, and a carbon of 30 ppm.

Endurance Test

The results from the endurance test can be classified into two categories. The first concerns those parameters for which the test was instrumented - such as the temperature and pressure readings. These results have been covered adequately in the previous discussion. The second category consists of those results that were largely unpredictable from an analytical standpoint and which depended on the test for qualitative insights and quantitative data. These phenomena include the nature of the distortions of the convolutions and the shift in distribution of the LiF along the tube length. The following discussion deals with this second category of results.

A cursory inspection of the convolutions of the tubes and the radiographs initially suggested a correlation between LiF fullness and distortion. Certainly the inlet region showed very marked evidences of both. Further investigation, however, which included dimensional measurements of the convolutions and a careful removal of the convolution shell to inspect the frozen LiF within, suggests that the two phenomena - that of LiF fullness and extent of distortion - were probably due to separate mechanisms.

Convolution distortion appears to have taken place because of the insufficient local void volume available when passing from the solid to liquid phase. In this thesis an essential ingredient bringing about this condition within an individual convolution is that of gravity. The single convolution, tilted as it was during the test when the tube axis is oriented $21\frac{1}{2}^{o}$ from the vertical, enables gravity to exert force on the LiF to flow toward the "low" side, or toward the heat source. The consequence is that during the shade period, as the LiF starts freezing (and shrinking), the liquid tends to fill any developing void volume on the heater ("low") side of the convolution. The resulting distribution, as seen in the radiographs, shows a concentration of the LiF on the heater side of the convolution and much of the void on the "cold" side. When the shade period passes to the sun, melting takes place on the heater side where the void volume is limited. When the void volume is filled, further melting causes the convolution wall in that local sector to distort to accommodate the liquid LiF.

The convolution temperatures in figures 25 and 26 tend to confirm the above description. These figures plot the surface temperatures on the two instrumented convolutions (Nos. 3 and 9) that were distorted. The temperature at the top (nearest the heater) peak location is seen to pass through the melt temperature before that of any other location. Not only does this sector of the convolution reach melt temperature first, but its temperature is well into the melt region. Other sectors within the

same convolution remain within the frozen temperature region for much, if not all, of the total cycle. The apparent aberrations in some of the temperature curves may well be explained by the flow processes within the individual convolution as described previously.

LiF fullness, on the other hand, is brought about by the condition of incomplete melting of LiF within a convolution in addition to gravity. Incomplete melting in the first few convolutions was anticipated. Figure 32 shows the discrepancy between the heat input shown as broken lines and the potential for cooling if the convolution temperature was at 1122 K (1560^{o} F) shown as a solid line. Clearly, the first few convolutions were overcooled. At the end of the sun period, without the addition of LiF external to a convolution, we could expect void volume proportional to the salt not melted. The convolution temperature distribution (fig. 25(c)) does indicate, however, that the neck reaches melt temperature during the sun cycle. This would enable the molten LiF from the convolution above to flow down by gravity into the existing void volumes. The additional LiF to the convolution from above may be compensated to an extent by the loss of the molten LiF to the convolution below. The lowest convolution (No. 1) eventually approaches a condition of fullness where it cannot accept any additional amounts of LiF. Actually, a small amount will still enter to the extent that distortion (as described previously) has provided more total volume in the convolution. The next higher convolution thereafter approaches its condition of fullness as does the succeeding convolutions in sequence.

CONCLUDING REMARKS

The purpose of the three-tube tests was to obtain performance data and to gain an understanding of the mechanisms involved in transferring a radiant heat load to the flowing gas. While the sun-shade periods and the vacuum environment could be controlled or ascertained, the condition of zero-gravity obviously could not be attained. Although the design was selected to minimize the effect of operation in gravity, the physical results of the test were heavily influenced by the gravity effect. In an environment of zero or low gravity, a nonuniform distribution, resulting in a high concentration of LiF in some convolutions and totally void of LiF in others, to the extent encountered in the test, would not be expected. Given the condition of Earth gravity, however, the results herein should be regarded as having been obtained under a much more stringent circumstance than zero gravity.

After 2002 hours of testing, the tubes remained intact - no cracks in the niobium - 1-percent zirconium tubes and no leakage of LiF. The distortions were local. Equally important, the nonuniform distribution and distortions had little effect on the perform-

ance of the receiver tubes. With the last seven convolutions devoid of LiF, the tubes still functioned to heat helium-xenon, the working gas above the design temperature of 1089 K (1500° F) for most of the 96-minute cycle. The helium-xenon discharge temperature varied from 16 K (29° F) below to 28 K (50° F) above design. This represents a range of 6 percent below to 10 percent above the design temperature rise of the gas; or -1.5 to +2.5 percent variation from design absolute temperature.

There was some oxygen contamination of the niobium alloy throughout the length of the convoluted tubes but heaviest in the inlet region (2200 ppm in the fourth convolution). The source of the contamination has not been traced, but is suspected to be due to the factors peculiar to the test setup rather than to any source integral to the tube themselves. It is significant that with this level of contamination, the convolutions could still operate with distortion but without cracking or leaking.

The initial heat flux of the short-term test (full incident flux) and of the endurance test (with reflections and re-radiation) had to be reduced by 10 percent and 5 percent, respectively. These reductions substantiate the design intent of providing a margin of capability in the receiver. In the actual receiver, controllable doors would allow excess heat to radiate into space. This margin of capability is further enhanced if it is realized that the sun-shade periods selected for the test were based on minimum sun and maximum shade values. In an actual orbital mission, there would be generally a higher percentage of the sun period.

For flux input in the endurance test that was 95 percent of the full design value, the maximum convolution temperature was 1183 K (1670° F). This value is well within the limitation of the material.

If the question remains regarding what further steps can be taken so that LiF remains within each compartment, one answer would be to ensure that the LiF in the neck of each convolution is always solid (frozen). In this way, each convolution would have its original "allotment" of LiF to which nothing would be added or subtracted. If the LiF is properly distributed initially, the only way for overexpansion to occur is in the case of the average convoluted tube temperature reaching 1228 K (1750° F), the maximum temperature for which it was designed. One step toward accomplishing this end is to insert a niobium alloy collar around the neck of each convolution to form a barrier to the thermal radiation.

Lewis Research Center,
National Aeronautics and Space Administration,
Cleveland, Ohio, November 19, 1971,
112-27.

APPENDIX - TEST RESULTS ON THE CONVECTIVE COEFFICIENTS OF ARGON FLOWING THROUGH A TUBE WITH CIRCUMFERENTIALLY ROLLED GROOVES

The solar receiver tubes were designed to transfer the heat into the gas with the tube wall at the LiF melt temperature (1122 K (1560° F)). The following is the analysis of the convective coefficient required and the experimentation conducted to fulfull that requirement.

Based on the system specifications, the gas heat-transfer convective coefficient required was

$$h = \frac{WC_p \Delta T}{A(LMTD)}$$

$$= 86.3 \text{ W/(m}^2\text{)(K)}\left(15.2 \text{ Btu/(hr)(ft}^2\text{)(}^\circ\text{F)}\right)$$

where h is the gas-side convective coefficient, W is the gas flow rate, C_p is the specific heat of the gas, ΔT is the temperature rise of the gas, A is the surface area of heat transmission to the gas, and $LMTD$ is the log mean temperature difference between the heat-transfer area and the gas.

Defining a heat transfer factor:

$$j = \frac{h}{GC_p} (Pr)^{2/3}$$

a value $j = 0.0070$ was required where j is a nondimensional heat transfer factor, G is the gas flow rate per unit cross-sectional area, and Pr is the Prandtl number.

These values are approximately twice that obtained from flow through a plain tube. To increase the heat transfer, grooves were rolled circumferentially into a tube thereby promoting turbulence in the gas boundary layer. These "turbulators" were spaced 2.5 centimeters (1 in.) apart so that they could be alined within each convolution without affecting the functions of the LiF.

A test program was conducted to determine the depth of groove required. The apparatus and method used were virtually identical to those used for a test on internal fins (ref. 7). The test section is shown in figure 33.

Three groove depths were tested, 1.96 millimeter (0.077 in.), 1.42 millimeter (0.056 in.), and 1.12 millimeter (0.044 in.). They were tested with argon over a range of Reynolds numbers from 3300 to 12 000. The results are shown in figure 34. For

the j value of 0.0070 that was required and allowing a 10 percent higher margin, a groove depth of 1.24 millimeter (0.049 in.) was chosen.

The use of argon in the test determining proper groove depth raises the question of the test's applicability to helium-xenon. The Prandtl number of argon is above the minimum value (0.5) usually quoted for convection equations. Helium-xenon has a value of 0.27. An indication of the grooved tube test results to helium-xenon is shown in figure 35. This graph is the result of the steady-state points taken immediately before the first cycle of the long-term test. The abscissa is tube temperature - any one value representing a constant surface temperature throughout the tube. The ordinate is the gas discharge temperature as calculated from the difference in primary power readings with and without gas flow, at tube temperature levels of 867, 1006, 1102, and 1144 K (1100°, 1350°, 1525°, and 1600° F). The curves represent the theoretical gas discharge temperature based on h being equal to the design value of 86.3 watts per square meter per K (15.2 Btu/(hr)(ft^2)($^{\circ}$F)) and to a value 10 percent higher than design, 94.8 watts per square meter per K (16.7 Btu/(hr)(ft^2)($^{\circ}$F)).

The calculated gas temperatures are lower than the curves at low tube temperatures and higher at the high tube temperatures. Of particular significance is the condition at tube temperature of 867 K (1100° F). With 867 K (1100° F) gas entering, one would expect the gas discharge temperature to be 867 K (1100° F). The calculated gas temperature, however, is lower than the tube temperature. This means that the power input under the no-flow condition required greater power to maintain the 867 K (1100° F) tube temperature than under the flow condition. The reason for this apparent incongruity is the heat loss out of the test section by conduction along the tubes. Under a no-flow condition, the end heat loss is eventually radiated to the environment. With flow, however, the preheated gas at 867 K (1100° F) compensates for the heat loss and requires less power from within the test section. In terms of figure 35 a more equal condition of end heat loss (for the flow and no-flow cases) at 867 K (1100° F) would result in an increase of gas temperature toward 867 K (1100° F). At a tube temperature of 1144 K (1600° F), however, the end heat loss with flow is due not only to radiation to the surroundings but due to convective loss to the incoming gas as well. Higher power for flow is required, therefore, to compensate for the end effect. Any effect in making the end losses more equal for the 1144 K (1600° F) tube temperature case would tend to decrease the calculated gas temperature. Intermediate tube temperatures would show effects somewhere between the two extremes. The foregoing discussion lends veracity to the values of h shown. It indicates, further, that values determined by an experimental test with argon (Pr = 0.67) are applicable to helium-xenon (Pr = 0.27) within the constraints common to both tests.

REFERENCES

1. Burns, Raymond K.: Preliminary Thermal Performance Analysis of the Solar Brayton Heat Receiver. NASA TN D-6268, 1971.

2. McKinnon, R. A.; and Kamperman, E. F.: Sunflower Boiler/Heat Storage. Rep. ER-4869, TRW, Inc. (NASA CR-51339), Apr. 1963.

3. McKinnon, R. A.; Vild, T. J.; and Milko, J. A.: Design Study of Solar Absorbers with Lithium Fluoride Heat Storage. Space Power Systems Engineering. G. C. Szego and J. E. Taylor, eds., Academic Press, 1966, pp. 795-820.

4. Anon.: Brayton Cycle Cavity Receiver Design Study. Rep. ER-6497, TRW, Inc. (NASA CR-54752), Nov. 22, 1965.

5. Schrenk, G. L.; and Gritton, D. G.: Analysis of Solar Reflectors. Mathematical Theory and Methodology for Simulation of Real Reflectors. Rep. EDR-3693, Allison Div., General Motors Corp., Dec. 16, 1963. (Available from DDC as AD-602870.)

6. Hoffman, E. E.; and Holowach, J.: The Cb-1Zr Rankine System Corrosion Test Loop. NASA CR-1509, 1970.

7. Namkoong, David; and Lynch, Michael P.: Experimental Results of Heat Transfer and Pressure Drop of Argon Flowing through Single Tube with Internal Interrupted Fins. NASA TM X-1428, 1967.

TABLE I. - DIMENSIONS OF RECEIVER TUBE NUMBER 1 BEFORE TEST[a]

(a) All measurements in centimeters

Convolution	Dimension								
	A		B		C		D		
	Orientation, deg								
	90 - 270	0 - 180	90 - 270	0 - 180	90	270	90	270	Average
[b]1	8.354	8.341	3.378	3.378	2.46	2.49	1.628	1.636	1.631
2	8.372	8.372	3.371	3.378	4.95	4.93	1.603	1.623	1.613
3	8.379	8.390	3.376	3.386	7.42	7.44	1.608	1.621	1.615
4	8.377	8.374	3.386	3.383	9.93	9.86	1.603	1.618	1.610
5	8.372	8.359	3.388	3.388	12.45	12.32	1.621	1.610	1.615
6	8.382	8.395	3.393	3.391	14.94	14.91	1.638	1.618	1.628
7	8.320	8.311	3.386	3.383	17.37	17.27	1.562	1.580	1.570
8	8.161	8.177	3.381	3.386	19.76	19.74	1.473	1.486	1.478
9	8.092	8.082	3.391	3.378	22.22	22.20	1.547	1.554	1.549
10	7.978	7.973	3.383	3.391	24.74	24.71	1.590	1.587	1.590
11	7.861	7.874	3.381	3.383	27.20	27.15	1.488	1.496	1.494
12	7.883	7.883	3.373	3.378	29.57	29.57	1.488	1.491	1.488
13	7.645	7.656	3.365	3.378	32.05	32.03	1.398	1.392	1.394
14	7.562	7.556	3.381	3.376	34.44	34.47	1.468	1.488	1.478
15	7.455	7.462	3.366	3.376	36.90	36.96	1.491	1.509	1.497
16	7.343	7.336	3.358	3.363	39.34	39.42	1.435	1.438	1.438
17	7.236	7.219	3.371	3.363	41.78	41.88	1.412	1.407	1.410
18	7.168	7.155	3.381	3.378	44.25	44.30	1.493	1.473	1.483
19	7.018	7.028	3.373	3.378	46.63	46.74	1.445	1.440	1.443
20	6.942	6.944	3.383	3.378	49.10	49.23	1.468	1.455	1.463
21	6.843	6.848	3.381	3.383	51.59	51.71	1.494	1.483	1.488
22	6.701	6.718	3.371	3.378	54.00	54.10	1.412	1.391	1.402
23	6.609	6.604	3.376	3.363	56.46	56.54	1.394	1.377	1.387
24	6.525	6.530	3.365	3.373	58.90	59.00	1.410	1.405	1.407
25	6.429	6.426	3.368	3.381	61.32	61.42	1.453	1.417	1.435
26	6.319	6.322	3.381	3.371	63.78	63.91	1.407	1.397	1.402
27	6.236	6.213	3.376	3.383	66.24	66.34	1.384	1.377	1.382
28	6.129	6.129	3.363	3.360	68.78	68.76	1.435	1.392	1.412
29	6.036	6.043	3.363	3.373	71.27	71.25	1.410	1.388	1.340
30	5.921	5.916	3.373	3.368	73.76	73.74	1.412	1.427	1.420
31	5.837	5.842	3.371	3.373	76.25	76.25	1.471	1.499	1.483
32	5.707	5.710	3.358	3.376	78.74	78.74	1.478	1.445	1.463
33	5.639	5.636	3.355	3.368	81.23	81.23	1.501	1.493	1.499
34	5.541	5.555	3.368	3.358	83.72	83.72	1.524	1.491	1.509
35	5.443	5.428	3.378	3.373	86.21	86.26	1.565	1.562	1.565
36	5.301	5.296	3.383	3.373	88.77	88.77	1.486	1.504	1.493
[c]37	5.220	5.237	-----	-----	-----	-----	1.519	1.430	1.463

[a]Dimensions are shown in fig. 7.

[b]Gas inlet.

[c]Gas discharge.

TABLE I. - Concluded. DIMENSIONS OF RECEIVER TUBE

NUMBER 1 BEFORE TEST[a]

(b) All measurements in inches

Convolution	Dimension								
	A		B		C		D		
	Orientation, deg								
	90 - 270	0 - 180	90 - 270	0 - 180	90	270	90	270	Average
[b]1	3.289	3.284	1.330	1.330	0.97	0.98	0.641	0.644	0.642
2	3.296	3.296	1.327	1.330	1.95	1.94	.631	.639	.635
3	3.299	3.303	1.329	1.333	2.92	2.93	.633	.638	.636
4	3.298	3.297	1.333	1.332	3.91	3.88	.631	.637	.634
5	3.296	3.291	1.334	1.334	4.90	4.85	.638	.634	.636
6	3.300	3.305	1.336	1.335	5.88	5.87	.645	.637	.641
7	3.274	3.272	1.333	1.332	6.84	6.80	.615	.622	.618
8	3.213	3.219	1.331	1.333	7.78	7.77	.580	.585	.582
9	3.186	3.182	1.335	1.330	8.75	8.74	.609	.612	.610
10	3.141	3.139	1.332	1.335	9.74	9.73	.626	.625	.626
11	3.095	3.100	1.331	1.332	10.71	10.69	.586	.589	.588
12	3.064	3.064	1.328	1.330	11.64	11.64	.586	.587	.586
13	3.010	3.014	1.325	1.330	12.62	12.61	.550	.548	.549
14	2.977	2.975	1.331	1.329	13.56	13.57	.578	.586	.582
15	2.935	2.938	1.325	1.329	14.53	14.55	.587	.594	.590
16	2.891	2.888	1.322	1.324	15.49	15.52	.565	.566	.566
17	2.849	2.842	1.327	1.324	16.45	16.49	.556	.554	.555
18	2.822	2.817	1.331	1.330	17.42	17.44	.588	.580	.584
19	2.763	2.767	1.328	1.330	18.36	18.40	.569	.567	.568
20	2.733	2.734	1.332	1.328	19.33	19.38	.578	.573	.576
21	2.694	2.696	1.331	1.332	20.31	20.36	.588	.584	.586
22	2.640	2.645	1.327	1.330	21.26	21.30	.556	.548	.552
23	2.602	2.600	1.329	1.324	22.23	22.26	.549	.542	.546
24	2.569	2.571	1.325	1.328	23.19	23.23	.555	.553	.554
25	2.531	2.530	1.326	1.331	24.14	24.18	.572	.558	.565
26	2.488	2.489	1.331	1.327	25.11	25.16	.554	.550	.552
27	2.455	2.446	1.329	1.332	26.08	26.12	.545	.542	.544
28	2.413	2.413	1.324	1.323	27.08	27.07	.565	.548	.556
29	2.377	2.379	1.324	1.328	28.06	28.05	.555	.547	.551
30	2.331	2.329	1.328	1.326	29.04	29.03	.556	.562	.559
31	2.298	2.300	1.327	1.328	30.02	30.02	.579	.590	.584
32	2.247	2.248	1.322	1.329	31.00	31.00	.582	.569	.576
33	2.220	2.219	1.321	1.326	31.98	31.98	.591	.588	.590
34	2.184	2.187	1.326	1.322	32.96	32.96	.600	.587	.594
35	2.143	2.137	1.330	1.328	33.94	33.96	.616	.615	.616
36	2.087	2.085	1.332	1.328	34.95	34.95	.585	.592	.588
[c]37	2.055	2.062	-----	-----	-----	-----	.598	.563	.576

[a]Dimensions are shown in fig. 7.

[b]Gas inlet.

[c]Gas discharge.

TABLE II. - DIMENSION OF RECEIVER TUBE NUMBER 2 BEFORE TEST[a]

(a) All measurements in centimeters

Convolution	Dimension								
	A		B		C		D		
	Orientation, deg								
	90 - 270	0 - 180	90 - 270	0 - 180	90	270	90	270	Average
[b]1	8.326	8.331	3.376	3.376	2.56	2.46	1.661	1.610	1.636
2	8.384	8.377	3.373	3.373	5.03	4.95	1.603	1.600	1.600
3	8.367	8.352	3.373	3.376	7.54	7.42	1.587	1.598	1.593
4	8.374	8.377	3.353	3.363	9.98	9.91	1.598	1.593	1.595
5	8.379	8.382	3.373	3.376	12.47	12.39	1.577	1.572	1.575
6	8.362	8.372	3.376	3.368	14.91	14.91	1.585	1.608	1.595
7	8.288	8.283	3.378	3.381	17.35	17.35	1.514	1.526	1.519
8	8.158	8.166	3.378	3.371	19.34	19.76	1.493	1.471	1.483
9	8.082	8.062	3.376	3.363	22.38	22.27	1.559	1.565	1.562
10	7.965	7.955	3.383	3.376	24.89	24.79	1.570	1.593	1.580
11	7.861	7.876	3.355	3.373	27.38	27.30	1.580	1.580	1.580
12	7.749	7.752	3.373	3.365	29.84	29.69	1.483	1.481	1.483
13	7.638	7.635	3.371	3.381	32.28	32.18	1.405	1.407	1.407
14	7.564	7.559	3.378	3.381	34.77	34.65	1.521	1.532	1.526
15	7.450	7.447	3.378	3.376	37.26	37.11	1.552	1.534	1.544
16	7.356	7.353	3.355	3.363	39.65	39.57	1.450	1.463	1.458
17	7.249	7.244	3.386	3.388	42.06	42.04	1.417	1.433	1.425
18	7.178	7.165	3.383	3.376	44.53	44.50	1.501	1.509	1.504
19	7.038	7.021	3.383	3.386	47.07	46.94	1.458	1.471	1.463
20	6.937	6.942	3.396	3.388	49.58	49.40	1.491	1.473	1.483
21	6.845	6.848	3.398	3.391	52.07	51.92	1.521	1.549	1.534
22	6.731	6.733	3.381	3.381	54.56	54.40	1.458	1.499	1.478
23	6.624	6.632	3.378	3.376	57.05	56.82	1.415	1.433	1.422
24	6.530	6.528	3.368	3.360	59.48	59.28	1.448	1.476	1.463
25	6.441	6.431	3.386	3.386	61.92	61.77	1.488	1.466	1.478
26	6.317	6.330	3.386	3.396	64.41	64.29	1.427	1.479	1.438
27	6.213	6.223	3.391	3.391	66.93	66.75	1.438	1.433	1.435
28	6.121	6.126	3.363	3.355	69.42	69.21	1.433	1.443	1.438
29	6.027	6.025	3.381	3.365	71.86	71.68	1.430	1.422	1.427
30	5.908	5.903	3.371	3.368	74.34	74.22	1.481	1.473	1.478
31	5.816	5.806	3.355	3.353	76.81	76.68	1.433	1.458	1.445
32	5.697	5.702	3.360	3.360	79.30	79.20	1.499	1.506	1.504
33	5.621	5.621	3.371	3.363	81.81	81.69	1.524	1.526	1.524
34	5.547	5.555	3.371	3.365	84.25	84.12	1.493	1.519	1.506
35	5.448	5.451	3.353	3.363	86.74	86.66	1.575	1.610	1.592
36	5.296	5.301	3.378	3.363	89.31	89.26	1.514	1.560	1.537
[c]37	5.222	5.248	-----	-----	-----	-----	1.463	1.486	1.473

[a]Dimensions are shown in fig. 7.

[b]Gas inlet.

[c]Gas discharge.

TABLE II. - Concluded. DIMENSIONS OF RECEIVER TUBE

NUMBER 2 BEFORE TEST[a]

(b) All measurements in inches

Convolution	Dimension								
	A		B		C		D		
	Orientation, deg								
	90 - 270	0 - 180	90 - 270	0 - 180	90	270	90	270	Average
[b]1	3.278	3.280	1.329	1.329	1.01	0.97	0.654	0.634	0.644
2	3.301	3.298	1.328	1.328	1.98	1.95	.631	.630	.630
3	3.294	3.288	1.328	1.329	2.97	2.92	.625	.629	.627
4	3.297	3.298	1.320	1.324	3.93	3.90	.629	.627	.628
5	3.299	3.300	1.329	1.328	4.91	4.88	.621	.619	.620
6	3.292	3.296	1.329	1.326	5.87	5.87	.624	.633	.628
7	3.263	3.261	1.330	1.331	6.83	6.83	.596	.601	.598
8	3.212	3.215	1.330	1.327	7.81	7.78	.588	.579	.584
9	3.182	3.174	1.329	1.324	8.81	8.77	.614	.616	.615
10	3.136	3.132	1.332	1.329	9.80	9.76	.618	.627	.622
11	3.095	3.101	1.321	1.328	10.78	10.75	.622	.622	.622
12	3.051	3.052	1.328	1.325	11.75	11.69	.584	.583	.584
13	3.007	3.006	1.327	1.331	12.71	12.67	.553	.554	.554
14	2.978	2.976	1.330	1.331	13.69	13.64	.599	.603	.601
15	2.933	2.932	1.330	1.329	14.67	14.61	.611	.604	.608
16	2.896	2.895	1.321	1.324	15.61	15.58	.571	.576	.574
17	2.854	2.852	1.333	1.334	16.56	16.55	.558	.564	.561
18	2.826	2.821	1.332	1.329	17.53	17.52	.591	.594	.592
19	2.771	2.764	1.332	1.333	18.53	18.48	.574	.579	.576
20	2.731	2.733	1.337	1.334	19.52	19.45	.587	.580	.584
21	2.695	2.696	1.338	1.335	20.50	20.44	.599	.610	.604
22	2.650	2.651	1.331	1.331	21.48	21.42	.574	.590	.582
23	2.608	2.611	1.330	1.329	22.46	22.37	.557	.564	.560
24	2.571	2.570	1.326	1.323	23.42	23.34	.570	.581	.576
25	2.536	2.532	1.333	1.333	24.38	24.32	.586	.577	.582
26	2.487	2.492	1.333	1.337	25.36	25.31	.562	.570	.566
27	2.446	2.450	1.335	1.335	26.35	26.28	.566	.564	.565
28	2.410	2.412	1.324	1.321	27.33	27.25	.564	.568	.566
29	2.373	2.372	1.331	1.325	28.29	28.22	.563	.560	.562
30	2.326	2.324	1.327	1.326	29.27	29.22	.583	.580	.582
31	2.290	2.286	1.321	1.320	30.24	30.19	.564	.574	.569
32	2.243	2.245	1.323	1.323	31.22	31.18	.590	.593	.592
33	2.213	2.213	1.327	1.324	32.21	32.16	.600	.601	.600
34	2.184	2.187	1.327	1.325	33.17	33.12	.588	.598	.593
35	2.145	2.146	1.320	1.324	34.15	34.12	.620	.634	.627
36	2.085	2.087	1.330	1.324	35.16	35.14	.596	.614	.605
37	2.056	2.066	-----	-----	-----	-----	.576	.585	.580

[a]Dimensions are shown in fig. 7.

[b]Gas inlet.

[c]Gas discharge.

TABLE III. - DIMENSIONS OF RECEIVER TUBE NUMBER 3 BEFORE TEST[a]

(a) All measurements in centimeters

Convolution	Dimension								
	A		B		C		D		
	Orientation, deg								
	90 - 270	0 - 180	90 - 270	0 - 180	90	270	90	270	Average
[b]1	8.334	8.321	3.378	3.383	2.49	2.41	1.626	1.620	1.623
2	8.340	8.387	3.378	3.370	4.90	4.85	1.597	1.615	1.605
3	8.395	8.387	3.388	3.383	7.34	7.29	1.593	1.620	1.605
4	8.387	8.379	3.376	3.381	9.83	9.83	1.603	1.651	1.626
5	8.402	8.395	3.381	3.383	12.29	12.19	1.595	1.618	1.605
6	8.392	8.395	3.386	3.386	14.71	14.71	1.590	1.603	1.590
7	8.308	8.316	3.378	3.370	17.45	16.99	1.554	1.572	1.565
8	8.189	8.179	3.370	3.386	19.48	19.48	1.458	1.488	1.473
9	8.100	8.103	3.373	3.376	21.92	21.87	1.529	1.549	1.539
10	7.953	7.953	3.386	3.386	24.41	24.31	1.552	1.565	1.560
11	7.869	7.866	3.383	3.383	26.85	26.77	1.506	1.488	1.497
12	7.760	7.762	3.363	3.365	29.29	29.21	1.473	1.471	1.473
13	7.650	7.625	3.365	3.370	31.72	31.67	1.379	1.384	1.382
14	7.564	7.567	3.373	3.373	34.19	34.11	1.534	1.514	1.524
15	7.455	7.468	3.360	3.370	36.63	36.60	1.532	1.511	1.521
16	7.361	7.366	3.370	3.360	39.06	39.09	1.450	1.455	1.453
17	7.247	7.249	3.373	3.370	41.48	41.53	1.448	1.445	1.448
18	7.165	7.168	3.378	3.378	43.97	43.97	1.511	1.509	1.509
19	7.000	6.995	3.378	3.373	46.41	46.46	1.468	1.443	1.455
20	6.960	6.955	3.378	3.386	48.89	48.97	1.476	1.463	1.468
21	6.845	6.853	3.378	3.381	51.33	51.38	1.498	1.506	1.504
22	6.723	6.716	3.363	3.373	53.82	53.87	1.438	1.427	1.432
23	6.639	6.642	3.370	3.370	56.23	56.33	1.417	1.397	1.407
24	6.520	6.540	3.360	3.363	58.73	58.77	1.438	1.427	1.432
25	6.454	6.449	3.376	3.370	61.19	61.26	1.445	1.443	1.443
26	6.332	6.332	3.370	3.373	63.65	63.70	1.402	1.402	1.402
27	6.218	6.238	3.378	3.368	66.14	66.14	1.427	1.382	1.392
28	6.134	6.124	3.358	3.373	68.63	68.63	1.407	1.435	1.422
29	6.030	6.027	3.363	3.368	71.06	71.14	1.407	1.397	1.402
30	5.926	5.913	3.376	3.373	73.51	73.66	1.402	1.410	1.407
31	5.829	5.827	3.368	3.353	76.00	76.15	1.463	1.422	1.443
32	5.715	5.720	3.363	3.370	78.56	78.64	1.499	1.448	1.473
33	5.631	5.636	3.363	3.373	81.05	81.13	1.511	1.570	1.539
34	5.545	5.524	3.368	3.370	83.54	83.54	1.514	1.559	1.537
35	5.446	5.453	3.368	3.386	86.08	86.03	1.572	1.547	1.560
36	5.301	5.557	3.376	3.373	88.65	88.59	1.514	1.480	1.499
[c]37	5.222	5.237	-----	-----	-----	-----	1.435	1.435	1.435

[a]Dimensions are shown in fig. 7.

[b]Gas inlet.

[c]Gas discharge.

TABLE III. - Concluded. DIMENSIONS OF RECEIVER TUBE

NUMBER 3 BEFORE TEST[a]

(b) All measurements in inches

Convolution	Dimension								
	A		B		C		D		
	Orientation, deg								
	90 - 270	0 - 180	90 - 270	0 - 180	90	270	90	270	Average
[b]1	3.281	3.276	1.330	1.332	0.98	0.95	0.640	0.638	0.639
2	3.307	3.302	1.330	1.327	1.93	1.91	.629	.636	.632
3	3.305	3.302	1.334	1.332	2.89	2.87	.627	.638	.632
4	3.302	3.299	1.329	1.331	3.87	3.87	.631	.650	.640
5	3.308	3.305	1.331	1.332	4.84	4.80	.628	.637	.632
6	3.304	3.305	1.333	1.333	5.79	5.79	.626	.631	.626
7	3.271	3.274	1.330	1.327	6.75	6.69	.612	.619	.616
8	3.224	3.220	1.327	1.333	7.67	7.67	.574	.586	.580
9	3.189	3.190	1.328	1.329	8.63	8.61	.602	.610	.606
10	3.131	3.133	1.333	1.333	9.61	9.57	.611	.616	.614
11	3.098	3.097	1.332	1.332	10.57	10.54	.593	.586	.590
12	3.055	3.056	1.324	1.325	11.53	11.50	.580	.579	.580
13	3.011	3.002	1.325	1.327	12.49	12.47	.543	.545	.544
14	2.978	2.979	1.328	1.328	13.46	13.43	.604	.596	.600
15	2.935	2.940	1.323	1.327	14.42	14.41	.603	.595	.599
16	2.898	2.900	1.327	1.323	15.38	15.39	.571	.573	.572
17	2.853	2.854	1.328	1.327	16.33	16.35	.570	.569	.570
18	2.821	2.822	1.330	1.330	17.31	17.31	.595	.594	.594
19	2.756	2.754	1.330	1.328	18.27	18.29	.578	.568	.573
20	2.740	2.738	1.330	1.333	19.25	19.28	.581	.576	.578
21	2.695	2.698	1.330	1.331	20.21	20.23	.590	.593	.592
22	2.647	2.644	1.324	1.328	21.19	21.21	.566	.562	.564
23	2.614	2.615	1.327	1.327	22.14	22.18	.558	.550	.554
24	2.567	2.575	1.323	1.324	23.12	23.14	.566	.562	.564
25	2.541	2.539	1.329	1.327	24.09	24.12	.569	.568	.568
26	2.493	2.493	1.327	1.328	25.06	25.08	.552	.552	.552
27	2.448	2.456	1.330	1.326	26.04	26.04	.562	.544	.548
28	2.415	2.411	1.322	1.328	27.02	27.02	.554	.565	.560
29	2.374	2.373	1.324	1.326	27.98	28.01	.554	.550	.552
30	2.333	2.328	1.329	1.328	28.94	29.00	.552	.555	.554
31	2.295	2.294	1.326	1.320	29.92	29.98	.576	.560	.568
32	2.250	2.252	1.324	1.327	30.93	30.96	.590	.570	.580
33	2.217	2.219	1.324	1.328	31.91	31.94	.595	.618	.606
34	2.183	2.175	1.326	1.327	32.89	32.89	.596	.614	.605
35	2.144	2.147	1.326	1.333	33.89	33.87	.619	.609	.614
36	2.087	2.188	1.329	1.328	34.90	34.88	.596	.583	.590
[c]37	2.056	2.062	-----	-----	-----	-----	.565	.565	.565

[a]Dimensions are shown in fig. 7.

[b]Gas inlet.

[c]Gas discharge.

TABLE IV. - CHANGES IN DIMENSIONS OF RECEIVER TUBE NUMBER 1 AFTER TEST[a]

(a) All measurements are in centimeters

Convolution	Dimension									
	Measurement after test minus measurement before test								Measurement after test minus measurement averaged at 90° and 270° before test	
	ΔA		ΔB		ΔC		ΔD		ΔD'	
	Orientation, deg									
	90 - 270	0 - 180	90 - 270	0 - 180	90	270	90	270	0	180
[b]1	-0.058	-0.028	-0.013	-0.010	0.025	0.025	0.101	0.340	-0.010	0.450
2	-.048	-.041	.010	0	.025	.025	.190	.292	.119	.335
3	.008	0	.015	.005	.025	-.025	.013	.015	.023	.056
4	.020	.023	.005	.015	0	.051	.003	.010	.028	.005
5	.013	.015	.008	.010	.000	-.025	.015	.008	.010	.023
6	.013	.010	.003	.003	-.025	-.025	.031	.020	.046	.048
7	.013	.003	.005	.005	-.051	.051	.025	-.008	0	.013
8	.018	.015	.010	.008	.025	-.010	.003	-.018	-.005	.003
9	.008	.015	.005	.013	.025	0	.003	0	.013	.010
10	-.008	.003	.008	.003	-.051	0	.010	.018	-.005	.015
11	.013	-.008	.008	-.005	-.051	-.051	.008	.025	.013	.005
12	.010	-.005	.005	.003	.025	.025	.025	.008	.015	.008
13	-.003	-.008	.008	-.005	0	-.051	.046	.071	.046	.086
14	-.003	0	.003	.005	.051	.025	.041	.061	.043	.063
15	.013	-.003	.010	-.010	-.051	0	.013	.013	.003	-.010
16	-.010	.018	.003	.010	0	-.025	.005	.008	-.005	-.003
17	.010	.025	.005	.010	.025	0	.010	.008	.013	.005
18	.003	.003	.008	.010	0	.025	.003	.036	.003	.025
19	.005	0	.003	.008	0	0	-.013	.023	-.010	.005
20	.005	-.003	.003	.008	0	-.079	-.010	.010	-.015	0
21	.005	-.010	.005	-.003	-.051	-.101	.010	.013	.003	0
22	.005	-.008	.005	.008	0	.076	.013	.025	.018	.033
23	.008	.010	.005	.005	0	.051	-.008	.018	.018	.015
24	.000	-.010	.005	.005	0	-.101	-.003	.041	.066	.013
25	.003	.005	.008	.003	.025	.151	-.018	.051	.030	.018
26	.005	.005	.005	0	0	-.025	-.005	.023	.043	.005
27	.005	-.018	.003	.003	-.025	0	.003	.053	.041	.046
28	.003	.013	.005	.005	.025	0	.005	.025	.020	.010
29	0	-.005	.003	.003	.025	.025	.023	.059	.041	.036
30	.005	.005	.003	.005	-.051	-.025	.031	.038	.035	.015
31	-.003	.003	.003	-.005	.051	.025	-----	-----	-----	-----
32	0	0	.005	.010	0	0	-----	-----	-----	-----
33	0	.005	.005	-.005	-.025	-.051	-----	-----	-----	-----
34	.003	-.003	.000	.008	.025	.025	-----	-----	-----	-----
35	-.003	.025	.008	.005	.051	-.051	-----	-----	-----	-----
36	0	.005	0	.005	0	.076	-----	-----	-----	-----
[c]37	0	-.008	-----	-----	-----	-----	-----	-----	-----	-----

[a]Dimensions are shown in fig. 7.

[b]Gas inlet.

[c]Gas discharge.

TABLE IV. - Concluded. CHANGES IN DIMENSIONS OF RECEIVER TUBE NUMBER 1 AFTER TEST[a]

(b) All measurements are in inches

Convolution	Dimension									
	Measurement after test minus measurement before test								Measurement after test minus measurement averaged at 90° and 270° before test	
	ΔA		ΔB		ΔC		ΔD		ΔD'	
	Orientation, deg									
	90 - 270	0 - 180	90 - 270	0 - 180	90	270	90	270	0	180
[b]1	-0.023	-0.011	-0.005	-0.004	0.01	0.01	0.040	0.134	-0.004	0.177
2	-.019	-.016	.004	0	.01	.01	.075	.115	.047	.132
3	.003	0	.006	.002	.01	-.01	.005	.006	.009	.012
4	.008	.009	.002	.006	0	.02	.001	.004	.011	.002
5	.005	.006	.003	.004	0	-.01	.006	.003	.004	.009
6	.005	.004	.001	.001	-.01	-.01	.012	.008	.018	.019
7	.005	.001	.002	.002	-.02	.02	.010	-.003	0	.005
8	.007	.006	.004	.003	.01	-.04	.001	-.007	-.002	.001
9	.003	.006	.002	.005	.01	0	.001	0	.005	.004
10	-.003	.001	.003	.001	-.02	0	.004	.007	-.002	.006
11	.005	-.003	.003	-.002	-.02	-.02	.003	.010	.005	.002
12	.004	-.002	.002	.001	.01	.01	.010	.003	.006	.003
13	-.001	-.003	.003	-.002	0	-.02	.018	.028	.018	.034
14	-.001	0	.001	.002	.02	.01	.016	.024	.017	.025
15	.005	-.001	.004	-.004	-.02	0	.005	.005	.001	-.004
16	-.004	.007	.001	.004	0	-.01	.002	.003	-.002	-.001
17	.004	.010	.002	.004	.01	0	.004	.003	.005	.002
18	.001	.001	.003	.004	0	.01	.001	.014	.001	.010
19	.002	0	.001	.003	0	0	-.007	.009	-.004	.002
20	.002	-.001	.001	.003	0	-.03	-.004	.004	-.006	0
21	.002	-.004	.002	.001	-.02	-.04	.004	.005	.001	0
22	.002	-.003	.002	.003	0	.03	.005	.010	.007	.013
23	.003	.004	.002	.002	0	.02	-.003	.007	.007	.006
24	0	-.004	.002	.002	0	-.04	-.001	.016	.026	.005
25	.001	.002	.003	.001	.01	.06	-.007	.020	.012	.007
26	.002	.002	.002	0	0	-.01	-.002	.009	.017	.002
27	.002	-.007	.001	.001	-.01	0	.001	.021	.016	.018
28	.001	.005	.002	.002	.01	0	.002	.010	.008	.004
29	0	-.002	.001	.001	.01	.01	.009	.022	.016	.014
30	.002	.002	.001	.002	-.02	-.01	.012	.015	.014	.006
31	-.001	.001	.001	-.002	.02	.01	-----	-----	-----	-----
32	0	0	.002	.004	0	0	-----	-----	-----	-----
33	0	.002	.002	-.002	-.01	-.02	-----	-----	-----	-----
34	.001	-.001	0	.003	.01	.01	-----	-----	-----	-----
35	-.001	.010	.003	.002	.02	-.02	-----	-----	-----	-----
36	0	.002	0	.002	0	.03	-----	-----	-----	-----
[c]37	0	-.003	-----	-----	----	----	-----	-----	-----	-----

[a]Dimensions are shown in fig. 7.

[b]Gas inlet.

[c]Gas discharge.

TABLE V. - CHANGES IN DIMENSIONS OF RECEIVER TUBE NUMBER 2 AFTER TEST[a]

(a) All measurements in centimeters

Convolution	Dimension									
	Measurement after test minus measurement before test								Measurement after test minus measurement averaged at 90° and 270° before test	
	ΔA		ΔB		ΔC		ΔD		ΔD'	
	Orientation, deg									
	90 - 270	0 - 180	90 - 270	0 - 180	90	270	90	270	0	180
[b]1	-0.023	-0.046	0.003	-0.010	0.025	0.076	0.264	0.201	0.109	0.371
2	.008	0	.003	-.005	0	.025	0	.013	.033	.112
3	-.028	-.023	-.005	-.008	0	.076	.236	.198	.096	.388
4	-.038	-.038	-.003	-.010	.005	-.013	.206	.229	.211	.272
5	-.043	-.043	-.008	-.010	0	.025	.239	.221	.236	.262
6	-.030	-.041	-.015	-.005	-.025	0	.229	.185	.203	.236
7	-.030	-.041	-.015	-.005	-.025	.025	.236	.203	.221	.279
8	-.020	-.030	-.005	-.008	.051	0	.162	.147	.140	.229
9	-.013	-.018	-.015	-.013	-.025	0	.147	.147	.152	.282
10	-.010	0	-.003	-.015	0	-.051	.132	.119	.028	.279
11	0	-.015	-.003	-.018	-.025	-.051	.117	.079	-.008	.279
12	-.018	-.018	-.008	-.008	.025	.051	.102	.091	-.003	.279
13	-.038	-.038	.003	-.013	0	0	.145	.168	.165	.206
14	-.023	-.013	-.003	-.023		0	.122	.137	.079	.231
15	0	-.015	0	-.015		.008	.102	.104	.074	.239
16	0	-.013	.005	-.005		0	.086	.066	.066	.165
17	-.015	-.010	.003	-.008		0	.051	.045	.079	.160
18	.010	.003	-.005	0	.051	0	.056	.051	.038	.051
19	-.003	.005	-.005	.003	-.107	.025	.030	-.003	.020	.020
20	.005	.005	-.008	.003	-.025	-.051	.015	.020	.030	.013
21	.023	.005	.005	.003	.051	-.025	.015	.046	.008	.005
22	.010	.005	.003	.005	-.025	0	.030	-.015	-.008	-.013
23	.005	0	.005	.003	-.025	.051	.010	.003	.033	-.008
24	.008	-.003	.005	.005	0	0	.025	.020	.005	-.010
25	.015	.005	.005	.005	.051	0	-.010	.018	.010	-.025
26	.008	-.005	-.008	.003	-.051	.025	.008	.008	.003	.013
27	.010	.013	0	-.005	.051	.025	-.020	-.005	.010	-.041
28	.025	.008	.005	0	-.051	.025	.005	-.015	-.020	.008
29	.003	.005	-.005	.008	.025	.025	-.020	.008	-.010	-.013
30	.008	.008	.003	.003	0	-.076	-.048	-.028	.053	.036
31	.013	-.010	.003	.005	.025	.051	-----	-----	-----	-----
32	.008	-.003	.003	.005	-.025	-.025	-----	-----	-----	-----
33	.013	.010	.003	.008	-.051	.102	-----	-----	-----	-----
34	0	-.005	.008	.005	.025	.025	-----	-----	-----	-----
35	.003	-.005	.005	0	-.025	-.025	-----	-----	-----	-----
36	.010	.003	0	.010	-.025	.051	-----	-----	-----	-----
[c]37	.003	-.003	-----	-----	-----	-----	-----	-----	-----	-----

[a]Dimensions are shown in fig. 7.

[b]Gas inlet.

[c]Gas discharge.

TABLE V. - Concluded. CHANGES IN SIMENSIONS OF RECEIVER TUBE NUMBER 2 AFTER TEST[a]

(b) All measurements in inches

Convolution	Dimension									
	Measurement after test minus measurement before test								Measurement after test minus measurement averages at 90° and 270° before test	
	ΔA		ΔB		ΔC		ΔD		ΔD'	
	Orientation, deg									
	90 - 270	0 - 180	90 - 270	0 - 180	90	270	90	270	0	180
[b]1	-0.009	-0.018	0.001	-0.004	0.01	0.03	0.104	0.079	0.043	0.146
2	.003	0	.001	-.002	0	.01	.000	.005	.013	.044
3	-.011	-.009	-.002	-.003	0	.03	.093	.078	.038	.153
4	-.015	-.015	-.001	-.004	-.02	-.05	.081	.090	.083	.107
5	-.017	-.017	-.003	-.004	0	.01	.094	.087	.093	.103
6	-.012	-.016	-.006	-.002	-.01	0	.090	.073	.080	.093
7	-.012	-.016	-.006	-.002	-.01	.01	.093	.080	.087	.110
8	-.008	-.012	-.002	-.003	.02	0	.064	.058	.055	.090
9	-.005	-.007	-.006	-.005	-.01	0	.058	.058	.060	.111
10	-.004	0	-.001	-.006	.00	-.02	.051	.047	.011	.110
11	0	-.006	-.001	-.007	-.01	-.02	.046	.031	-.003	.110
12	-.007	-.007	-.003	-.003	.01	.02	.040	.036	-.001	.092
13	-.015	-.015	.001	-.005	0	0	.057	.066	.065	.081
14	-.009	-.005	-.001	-.009	↓	0	.048	.054	.031	.091
15	0	-.006	0	-.006	↓	.03	.040	.041	.029	.094
16	0	-.005	.002	-.002	↓	0	.034	.026	.026	.065
17	-.006	.004	.001	-.003	↓	0	.020	.018	.031	.063
18	.004	.001	-.002	0	.02	0	.022	.020	.015	.020
19	-.001	.002	-.002	.001	-.04	.01	.012	-.001	.008	.008
20	.002	.002	-.003	.001	-.01	-.02	.006	.008	.012	.005
21	.009	.002	.002	.001	.02	-.01	.006	.018	.003	.002
22	.004	.002	.001	.002	-.01	0	.012	-.006	-.003	-.005
23	.002	0	.002	.001	-.01	.02	.004	.001	.013	-.003
24	.003	-.001	.002	.002	0	0	.010	.008	.002	-.004
25	.006	.002	.002	.002	.02	0	-.004	.007	.004	-.010
26	.003	-.002	-.003	.001	-.02	.01	.003	.003	-.001	.005
27	.004	.005	0	-.002	.02	.01	-.008	-.002	.004	-.016
28	.010	.003	.002	0	-.02	.01	.002	-.006	-.008	.003
29	.001	.002	-.002	.003	.01	.01	-.008	.003	-.004	-.005
30	.003	.003	.001	0	0	-.03	-.019	-.011	-.021	-.014
31	.005	-.004	.001	.002	.01	.02	-----	-----	-----	-----
32	.003	-.001	.001	.002	-.01	-.01	-----	-----	-----	-----
33	.005	.004	.001	.003	-.02	.04	-----	-----	-----	-----
34	0	-.002	.003	.002	.01	.01	-----	-----	-----	-----
35	.001	-.002	.002	0	-.01	-.01	-----	-----	-----	-----
36	.004	.001	0	.004	-.01	-.02	-----	-----	-----	-----
[c]37	.001	-.001	-----	-----	----	----	-----	-----	-----	-----

[a]Dimensions are shown in fig. 7.
[b]Gas inlet.
[c]Gas discharge.

TABLE VI. - CHANGES IN DIMENSIONS OF RECEIVER TUBE NUMBER 3 AFTER TEST[a]

(a) All measurements in centimeteters

Convolution	Dimension									
	Measurement after test minus measurement before test								Measurement after test minus measurement averaged at 90° and 270° before test	
	ΔA		ΔB		ΔC		ΔD		ΔD'	
	Orientation, deg									
	90 - 270	0 - 180	90 - 270	0 - 180	90	270	90	270	0	180
[b]1	-0.045	-0.028	-0.005	0.003	0.051	0	0.312	0.224	0.068	0.386
2	.003	.003	.003	.003	0	0	.323	.010	.008	.114
3	.010	-.003	.010	-.003	.025	-.025	.053	.028	.013	.091
4	.007	.013	.010	.013	-.102	.025	.079	.040	.046	.086
5	.013	.010	.013	.003	.051	.051	.038	.003	.028	.051
6	.013	.018	.010	.003	.025	0	.046	.033	.048	.071
7	.018	.018	.010	.008	0	0	.061	.053	.051	.076
8	.015	.015	.010	.005	.051	↓	.025	.023	.020	.041
9	.013	.013	.010	.013	-.076	↓	.003	-.010	-.005	-.010
10	.020	.015	.010	.008	.051	↓	.010	.015	.008	.010
11	.020	.013	.005	.008	-.051	-.025	.028	.010	.023	.013
12	.013	.010	.010	.008	.076	.025	.013	.010	.015	.013
13	.013	.010	.013	.010	-.025	.051	.010	.008	.008	.008
14	.013	.010	.008	.005	-.025	0	-.010	.005	.003	.005
15	.010	.007	.013	.008	-.051	↓	.008	.003	-.005	-.005
16	.008	.007	.008	.003	0	↓	-.008	-.003	-.010	.013
17	.010	.010	.003	.005	0	↓	-.010	-.003	-.018	.003
18	.008	.003	.005	.005	.025	-.025	.003	-.008	-.008	-.020
19	.005	.010	.008	.010	0	0	-.013	-.005	.005	-.030
20	.013	.008	.005	.005	-.025	-.051	.003	-.005	-.005	.008
21	.018	.008	.008	0	.025	.025	-.008	-.003	.008	-.005
22	.003	.013	.013	.003	-.025	.025	-.005	-.023	-.003	-.020
23	.007	.003	.005	.005	0	-.051	-.013	-.003	-.013	-.003
24	.008	.005	.005	.003	.025	0	.003	-.010	-.018	.013
25	.003	.005	.008	.003	.025	.025	.015	-.008	-.008	.028
26	.010	.005	.005	.005	0	.051	-.023	.020	-.018	.010
27	.008	.000	.005	.005	-.025	0	-.051	.036	.003	.015
28	.008	.010	.010	.005	-.051	-.025	-.018	-.038	-.025	-.038
29	.010	.005	.010	.008	.051	0	-.041	-.010	-.020	-.018
30	0	.005	.003	.005	.051	0	-.048	.025	-.008	-.023
31	.008	.005	.005	.005	.025	0	-----	-----	-----	-----
32	.008	.008	.005	-.003	-.051	.025	-----	-----	-----	-----
33	.008	.003	.008	.003	-.025	0	-----	-----	-----	-----
34	.013	.005	.008	.003	0	0	-----	-----	-----	-----
35	.008	.008	.002	-.003	-.025	.025	-----	-----	-----	-----
36	.008	.005	.000	0	.025	-.078	-----	-----	-----	-----
[c]37	-.008	.005	-----	-----	-----	-----	-----	-----	-----	-----

[a]Dimensions are shown in fig. 7.

[b]Gas inlet.

[c]Gas discharge.

TABLE VI. - Concluded. CHANGES IN DIMENSIONS OF RECEIVER TUBE NUMBER 3 AFTER TEST[a]

(b) All measurements in inches

Convolution	Dimension									
	Measurement after test minus measurement before test								Measurement after test minus measurement averaged at 90° and 270° before test	
	ΔA		ΔB		ΔC		ΔD		ΔD'	
	Orientation, deg									
	90 - 270	0 - 180	90 - 270	0 - 180	90	270	90	270	0	180
[b]1	-0.018	-0.011	-0.002	0.001	0.02	0	0.123	0.088	0.027	0.152
2	.001	.001	.001	.001	0	0	.127	.004	.003	.045
3	.004	-.001	.004	-.001	.01	-.01	.021	.011	.005	.036
4	.003	.005	.004	.005	-.04	.01	.031	.016	.018	.034
5	.005	.004	.005	.001	.02	.02	.015	.001	.011	.020
6	.005	.006	.004	.001	.01	0	.018	.013	.019	.028
7	.007	.006	.004	.003	0	0	.024	.021	.020	.030
8	.006	.006	.004	.002	.02	↓	.010	.009	.008	.016
9	.005	.005	.004	.005	-.03	↓	.001	-.004	-.002	-.004
10	.008	.006	.004	.003	.02	↓	.004	.006	.003	.004
11	.008	.005	.002	.003	-.02	-.01	.011	.004	.009	.005
12	.005	.004	.004	.003	.03	.01	.005	.004	.006	.005
13	.005	.004	.005	.004	-.01	.02	.004	.003	.003	.003
14	.005	.004	.003	.002	-.01	0	-.004	.002	.001	.002
15	.004	.003	.005	.003	-.02	↓	.003	.001	-.002	-.002
16	.003	.003	.003	.001	0	↓	-.003	-.003	-.004	.005
17	.004	.004	.001	.002	0	↓	-.004	-.001	-.007	.001
18	.003	.001	.002	.002	.01	-.01	.001	-.003	-.003	-.008
19	.008	.004	.003	.004	0	0	-.005	-.002	.002	-.012
20	.002	.003	.002	.001	-.01	-.02	.001	-.002	-.002	.003
21	.006	.003	.003	0	.01	.01	-.003	-.001	.003	-.002
22	.007	.005	.005	.001	-.01	.01	-.002	-.009	-.001	-.008
23	.001	.001	.002	.002	0	-.02	-.005	-.001	-.005	-.001
24	.003	.002	.002	.001	.01	0	.001	-.004	-.007	.005
25	.001	.002	.003	.001	.01	.01	.006	-.003	-.003	.011
26	.004	.002	.002	.002	0	.02	-.009	.008	-.007	.004
27	.003	0	.002	.002	-.01	0	-.020	.014	.001	.006
28	.003	.004	.004	.002	-.02	-.01	-.007	-.015	-.010	-.015
29	.004	.002	.004	.003	.02	0	-.016	-.004	-.008	-.007
30	0	.002	.001	.002	.02	0	-.019	.010	-.003	-.009
31	.003	.002	.002	.002	.01	0	-----	-----	-----	-----
32	.003	.003	.002	-.001	-.02	.01	-----	-----	-----	-----
33	.003	.001	.003	.001	-.01	0	-----	-----	-----	-----
34	.006	.002	.003	.001	0	0	-----	-----	-----	-----
35	.003	.003	.002	-.001	-.01	.01	-----	-----	-----	-----
36	.003	.002	0	0	.01	-.03	-----	-----	-----	-----
[c]37	-.003	.002	-----	-----	----	----	-----	-----	-----	-----

[a]Dimensions are shown in fig. 7.

[b]Gas inlet.

[c]Gas discharge.

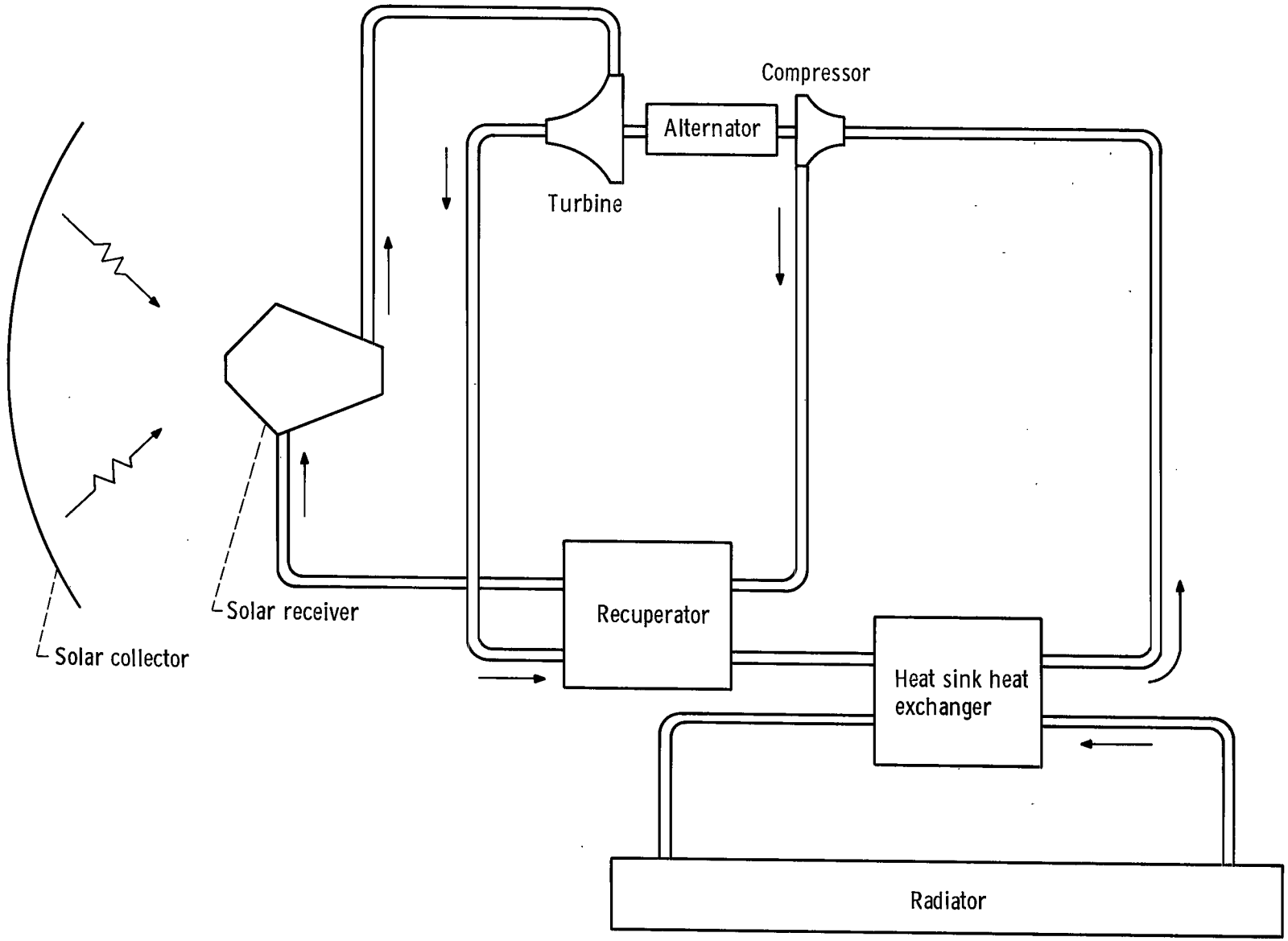

Figure 1. - Brayton solar-powered system.

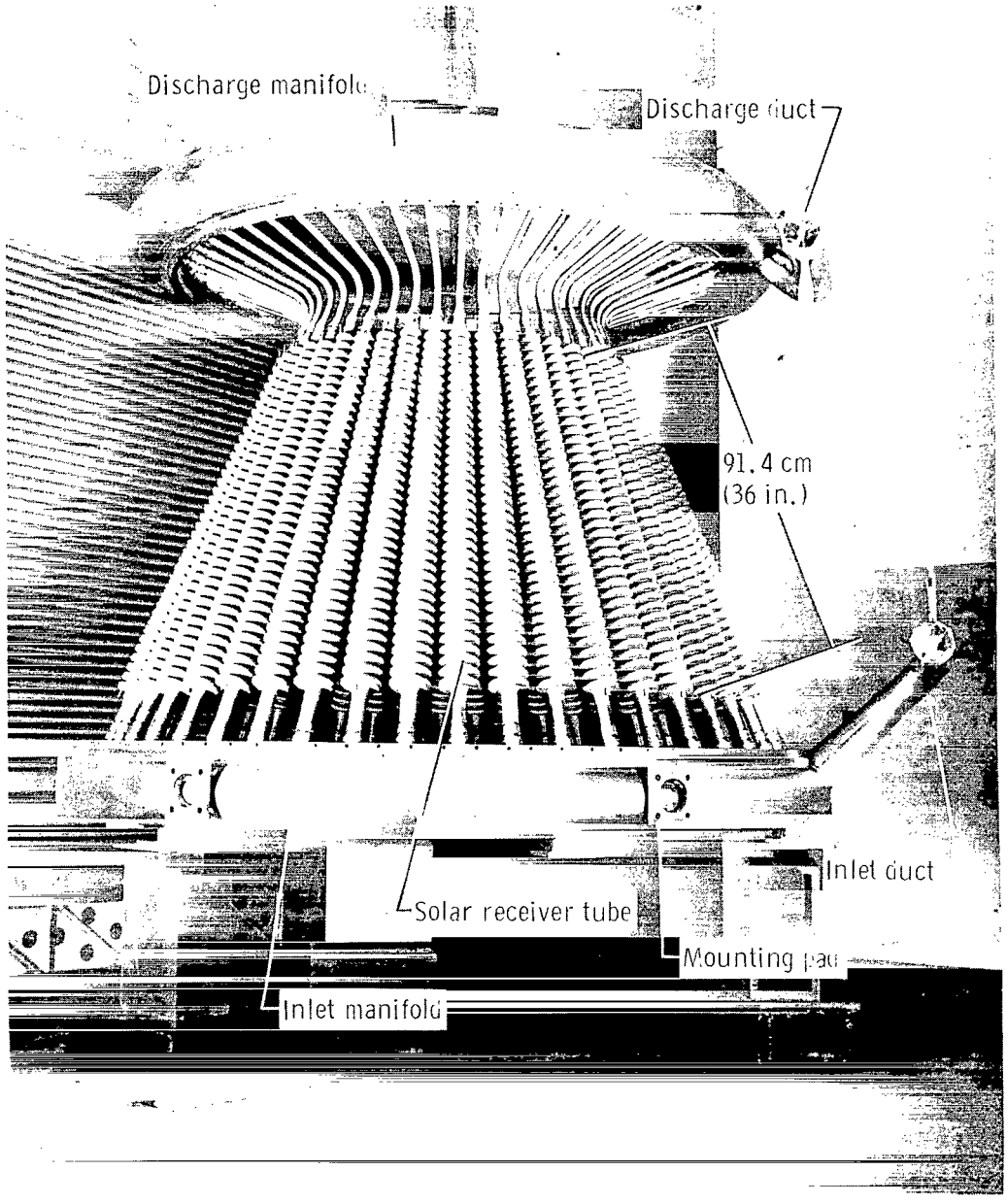

Figure 2. - Brayton cycle solar receiver without heat-reflector/insulator shell.

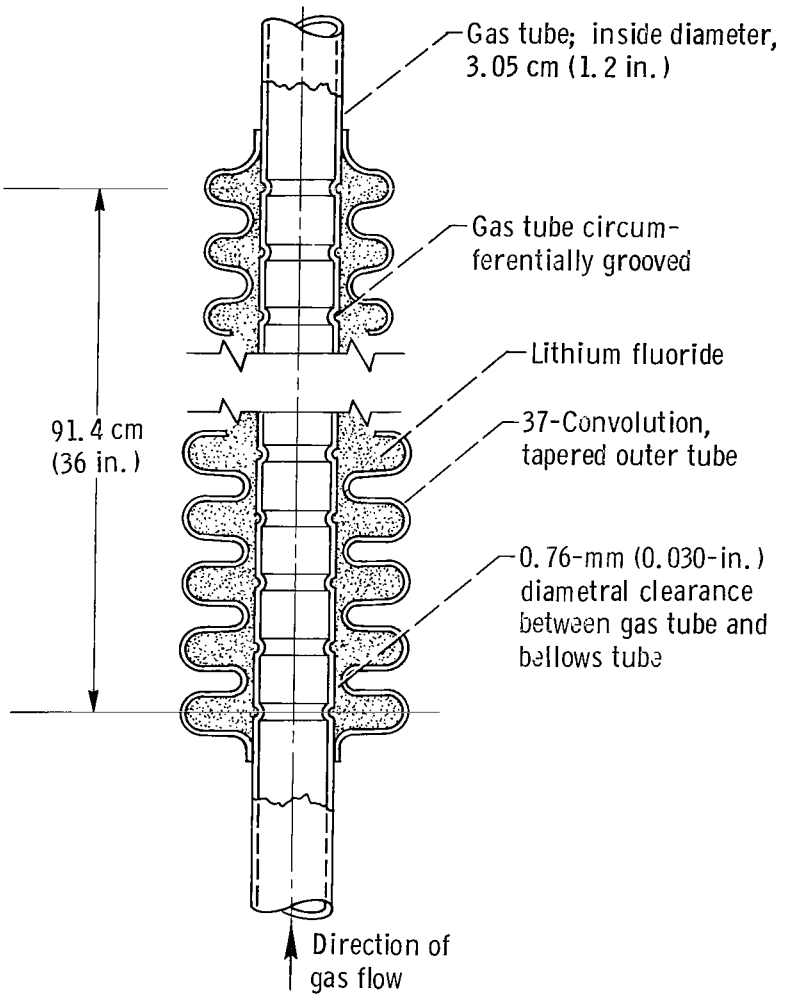

Figure 3. - Heat-transfer/heat-storage solar receiver tube.

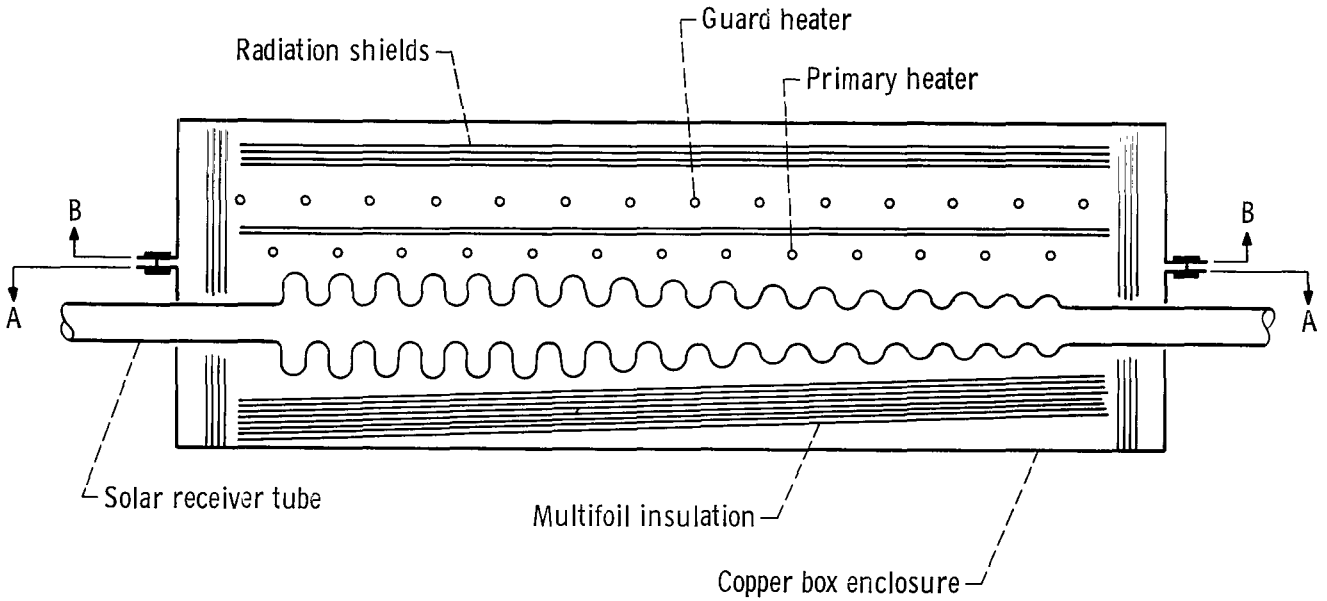

Figure 4. - Cross section through test section showing relative positions of contents. (For section A-A see fig. 5; for section B-B see fig. 6.)

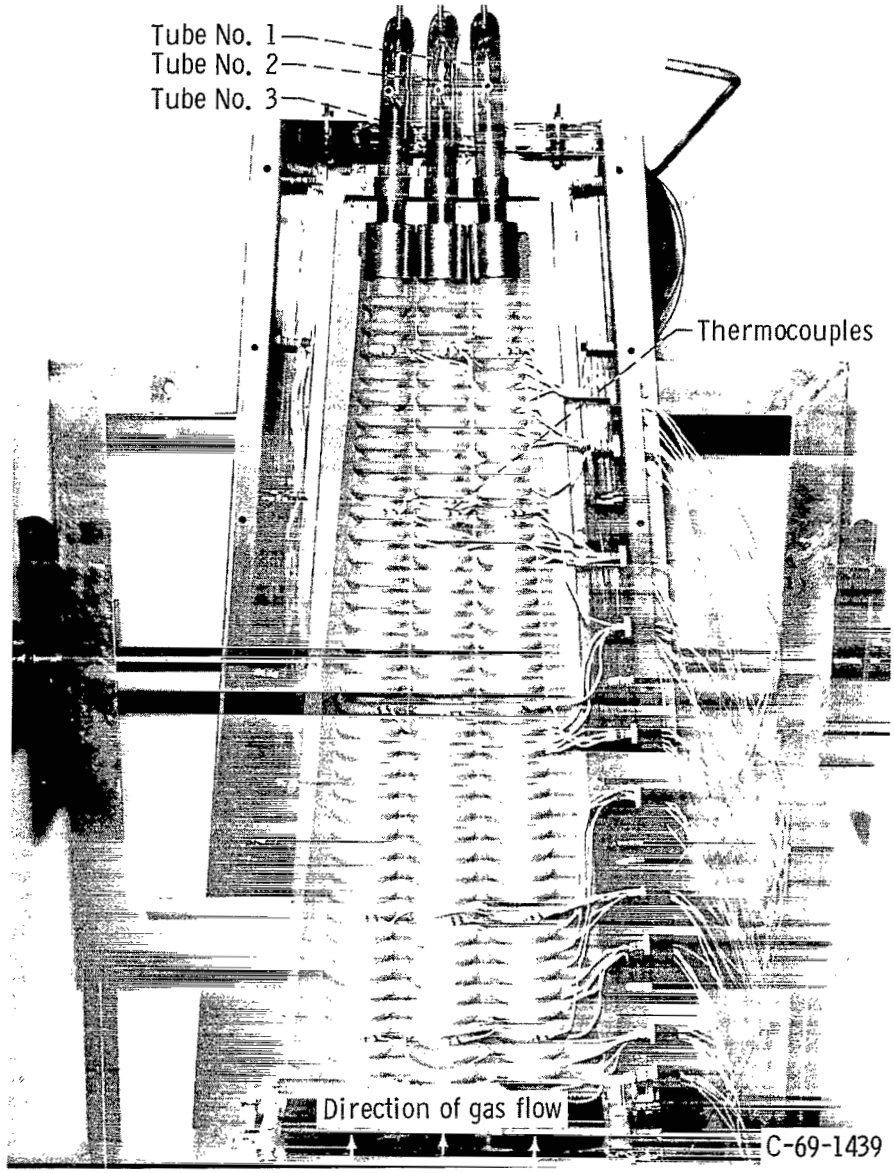

Figure 5. - Test section open showing receiver tubes in position.

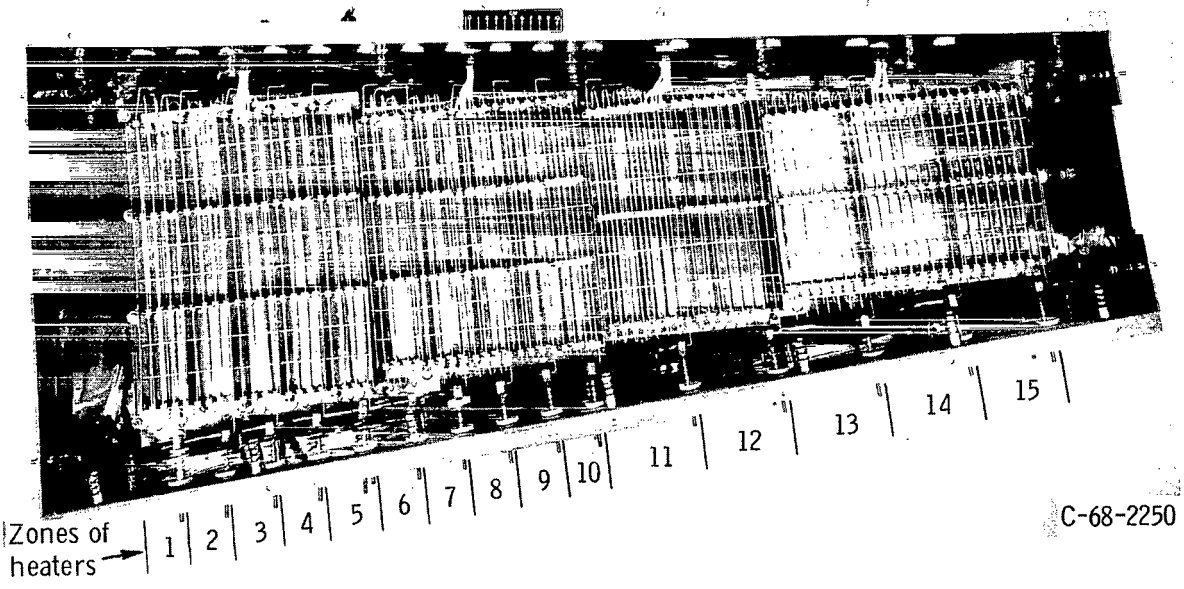

Figure 6. - Mating test section open showing tantalum wire heaters.

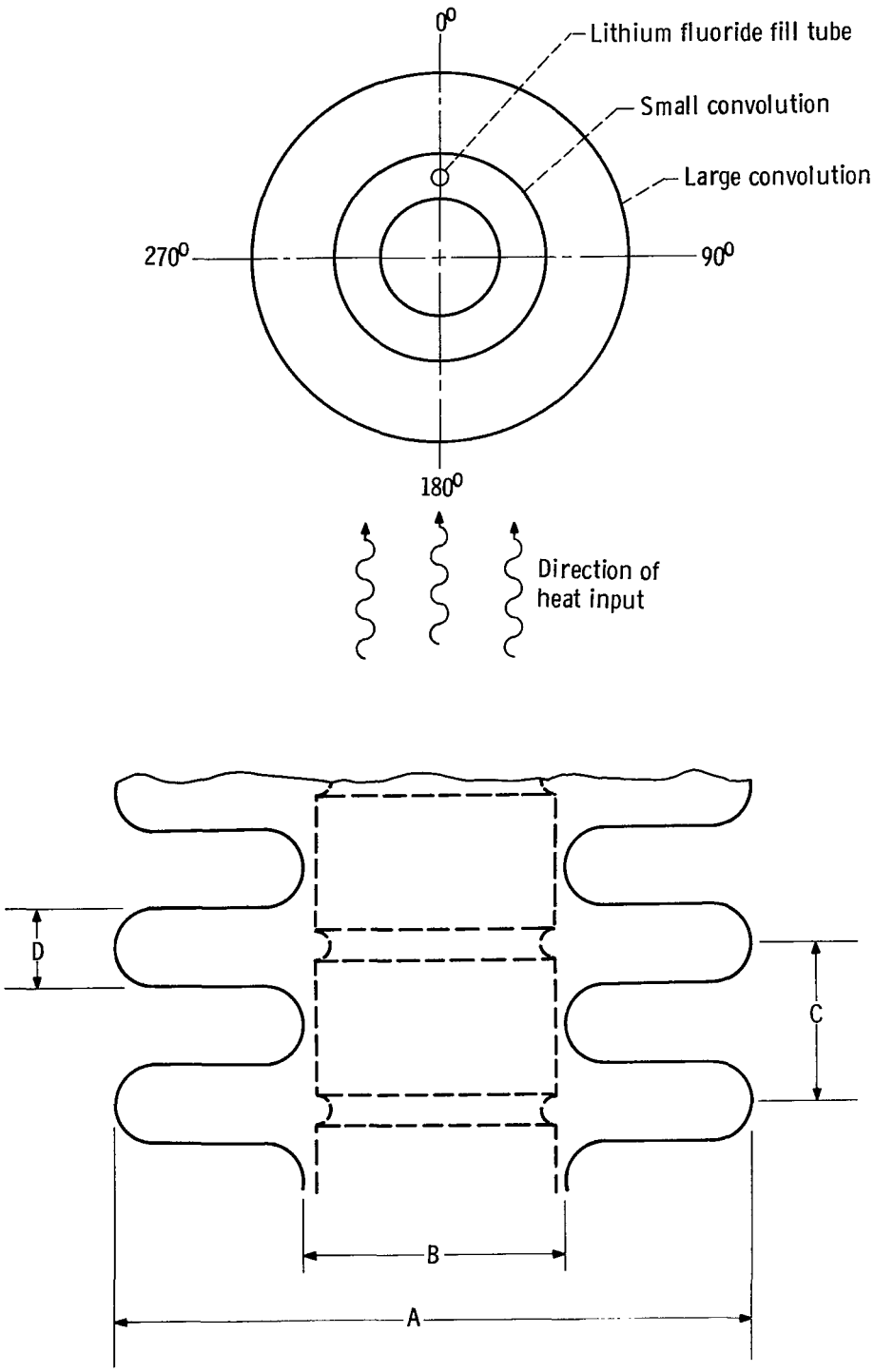

Figure 7. - Dimensions as tabulated in tables.

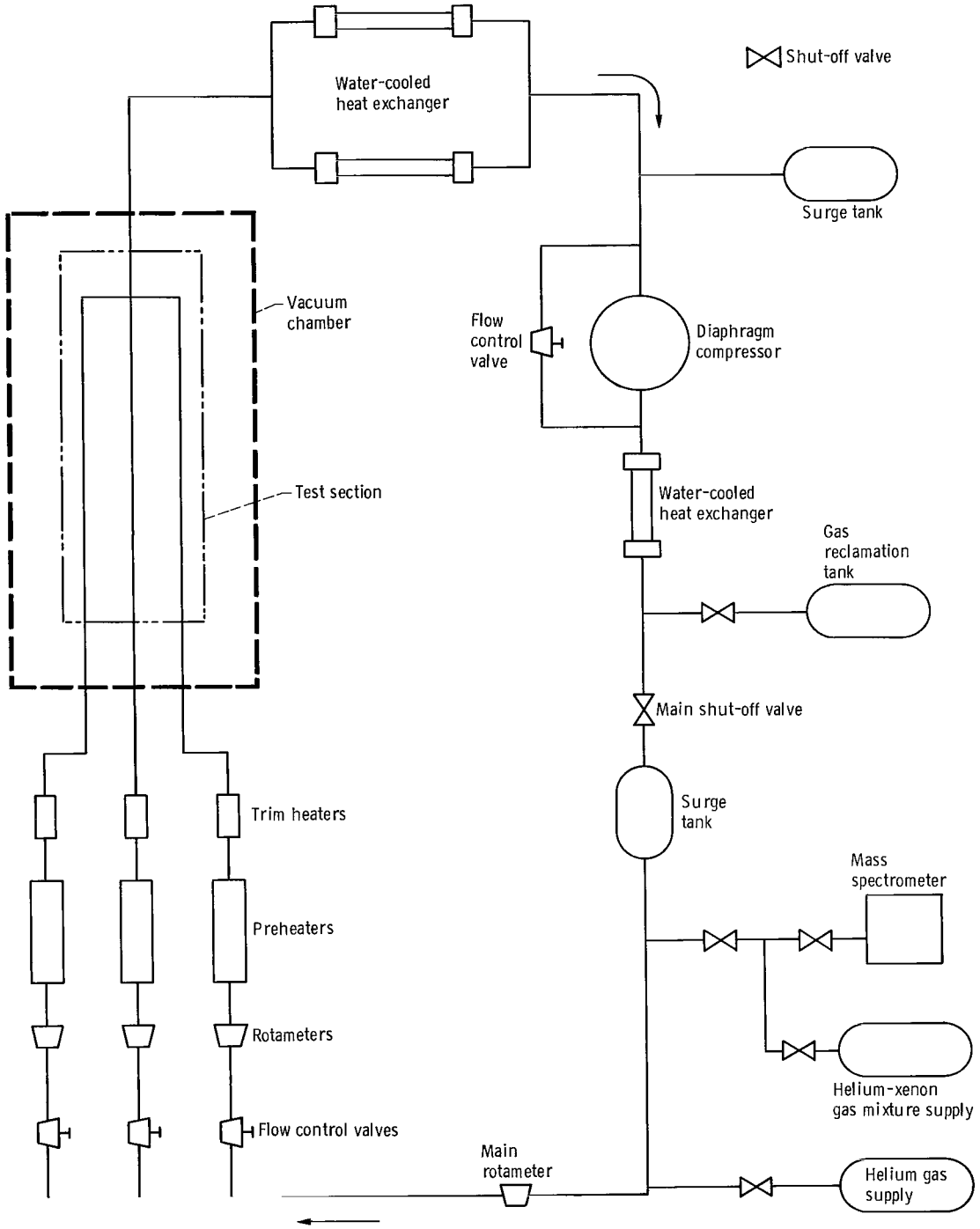

Figure 8. - Receiver tube test gas loop.

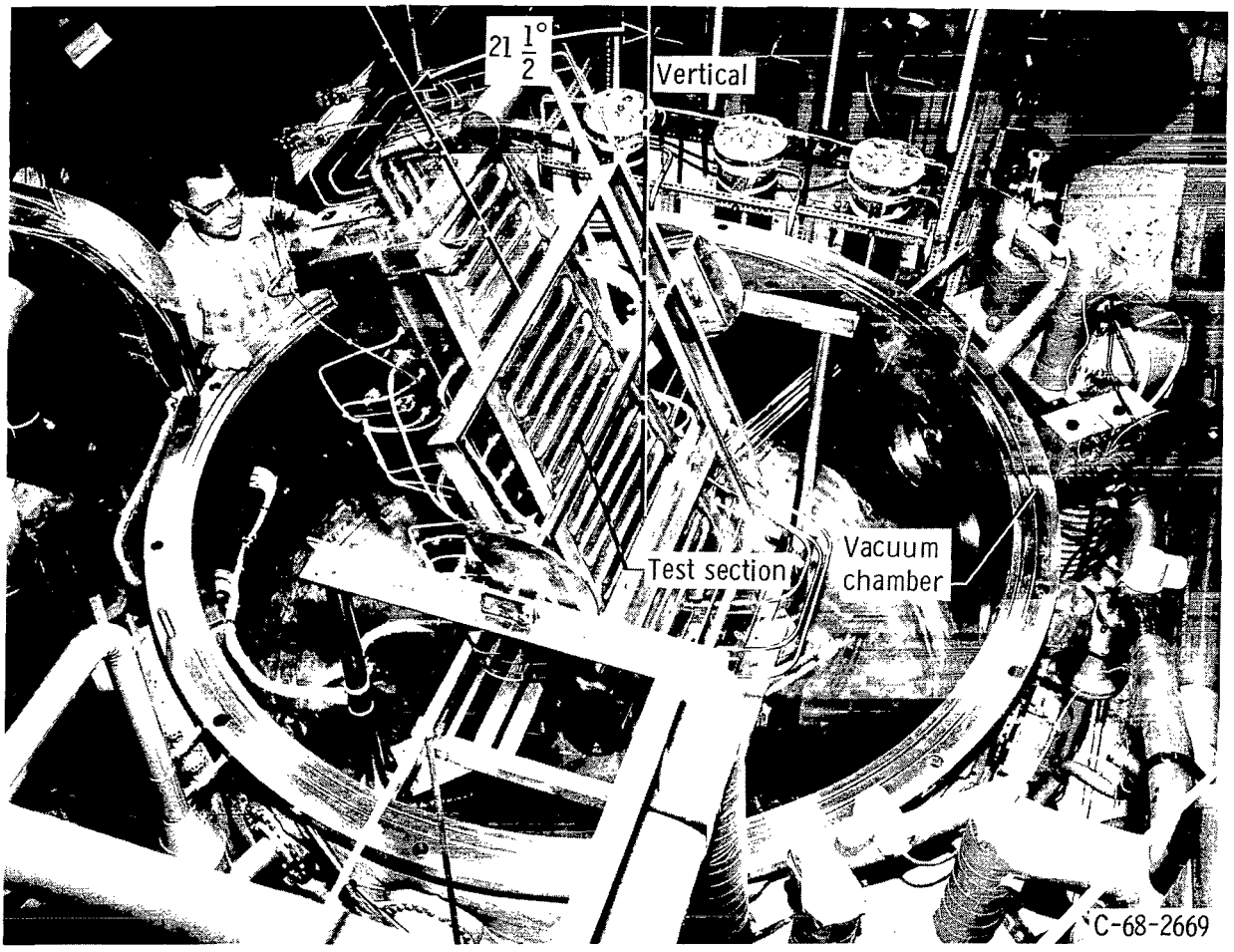

Figure 9. - Three-tube section in vacuum chamber.

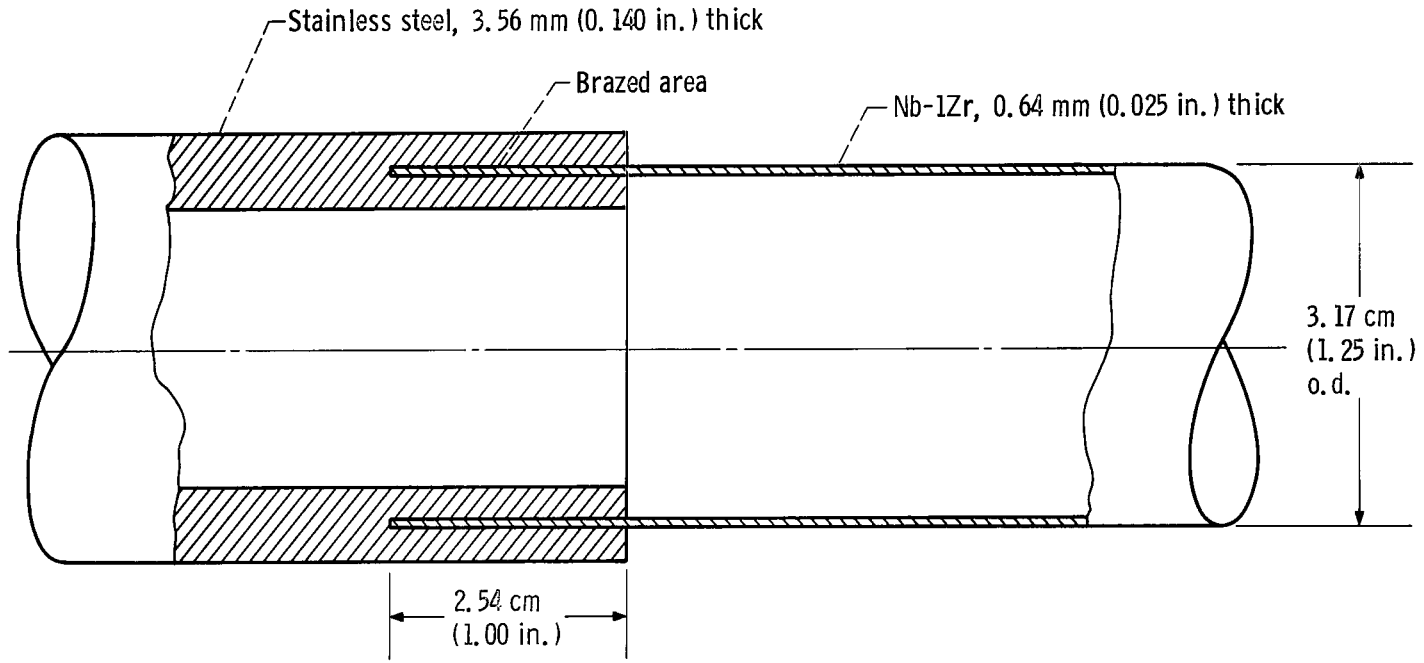

Figure 10. - Cross section of niobium-1-percent zirconium and stainless-steel bimetallic joint.

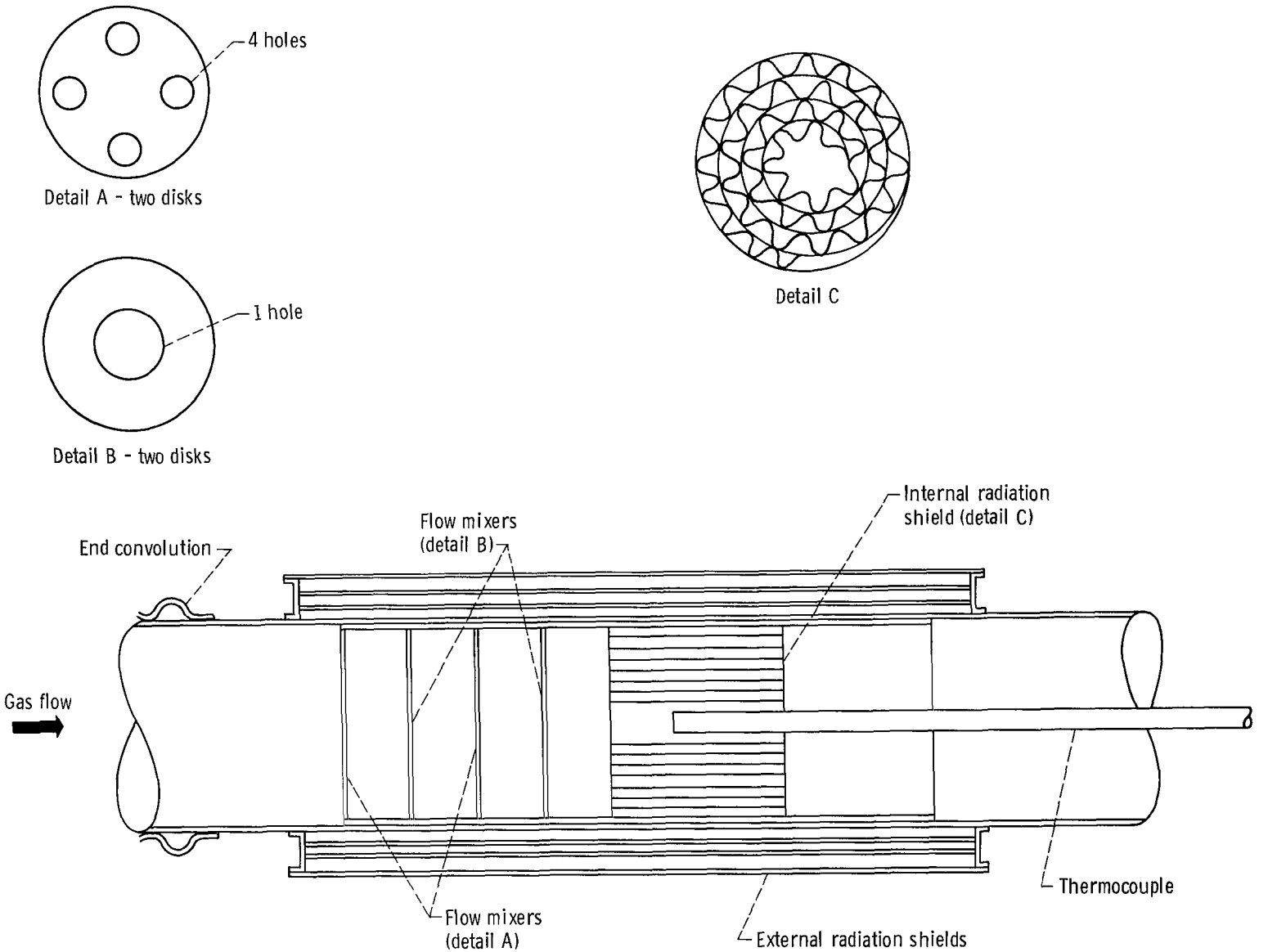

Figure 11. - Gas temperature measuring section.

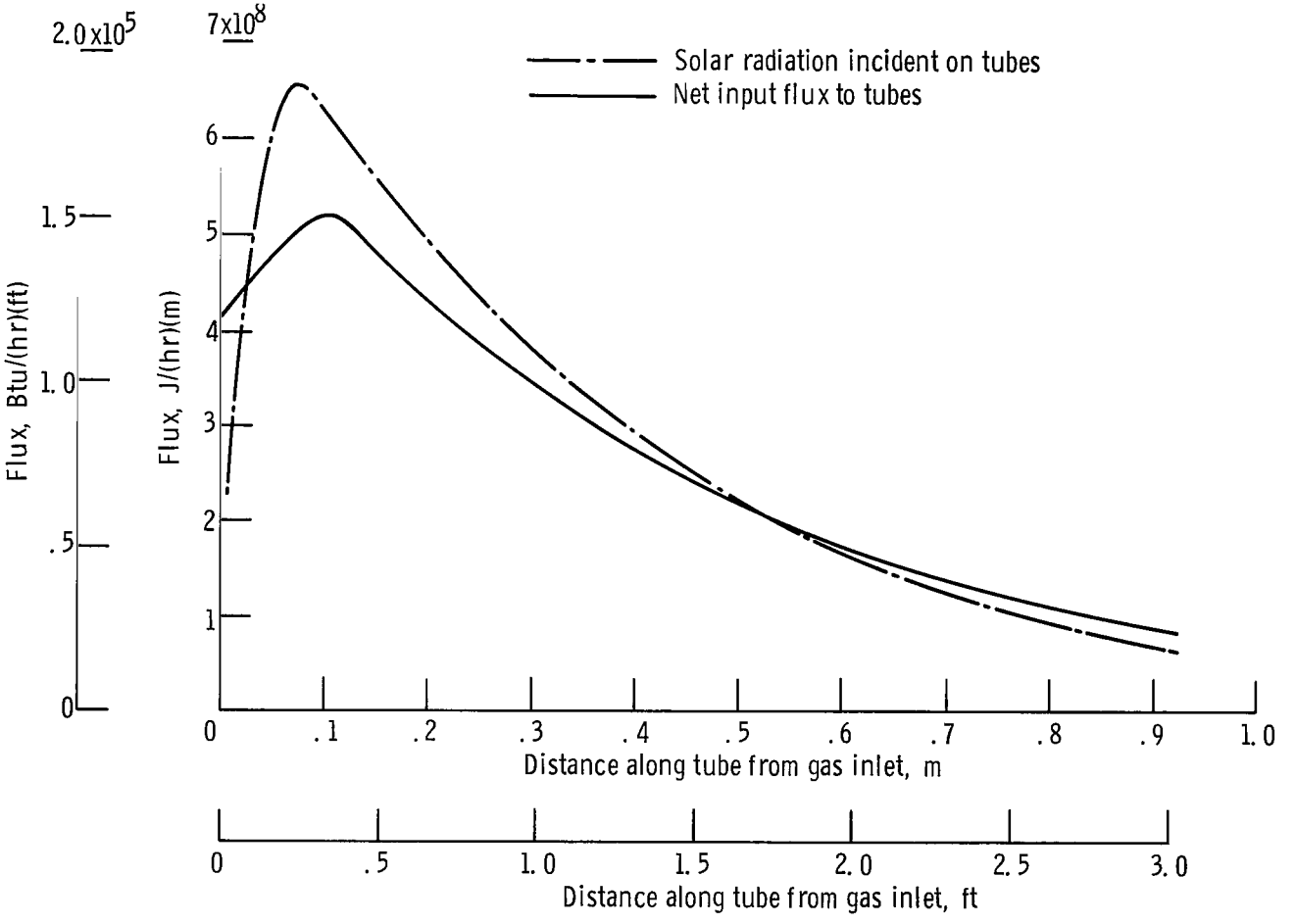

Figure 12. - Flux distributions along gas tube length.

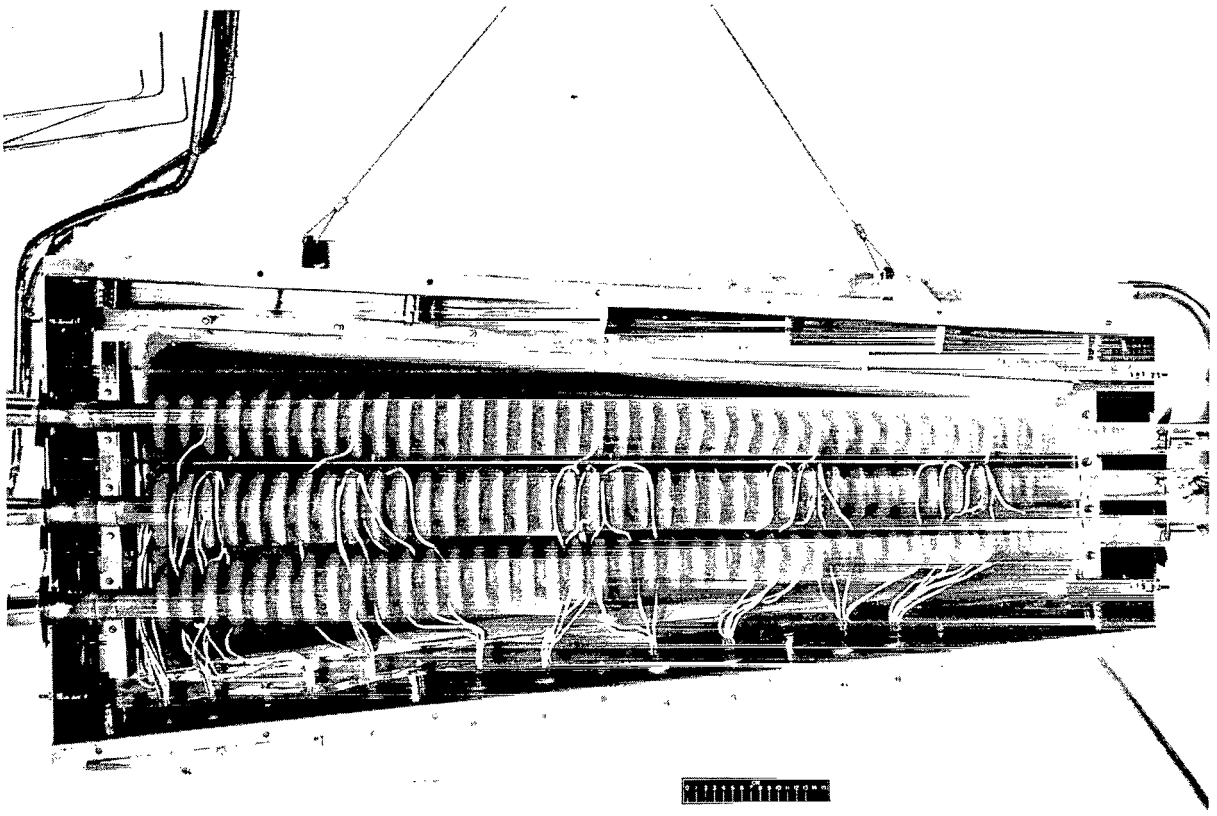

C-68-4080

Figure 13. - Iron titanate coated tubes after short-term test.

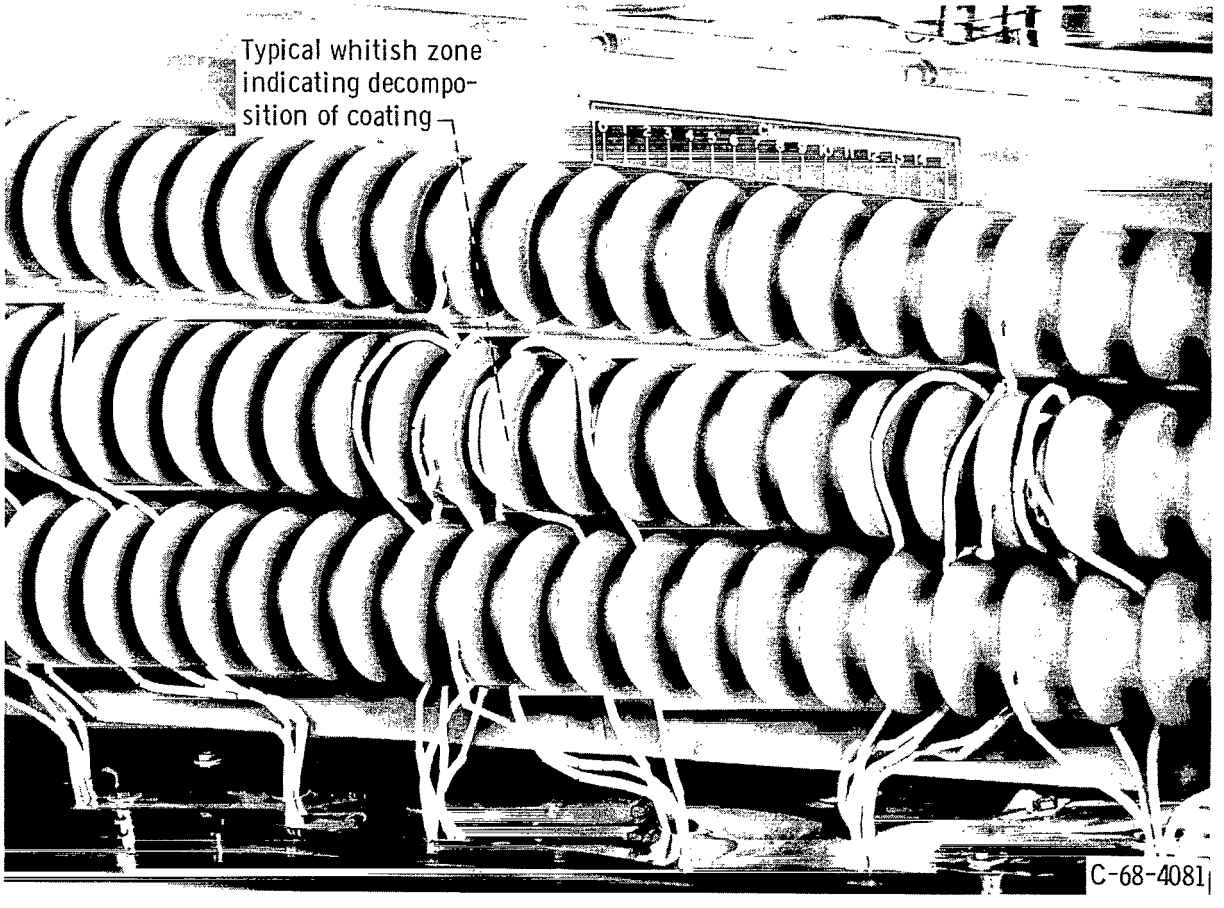

Figure 14. - Closeup of middle region of iron titanate coated receiver tubes showing decomposed areas.

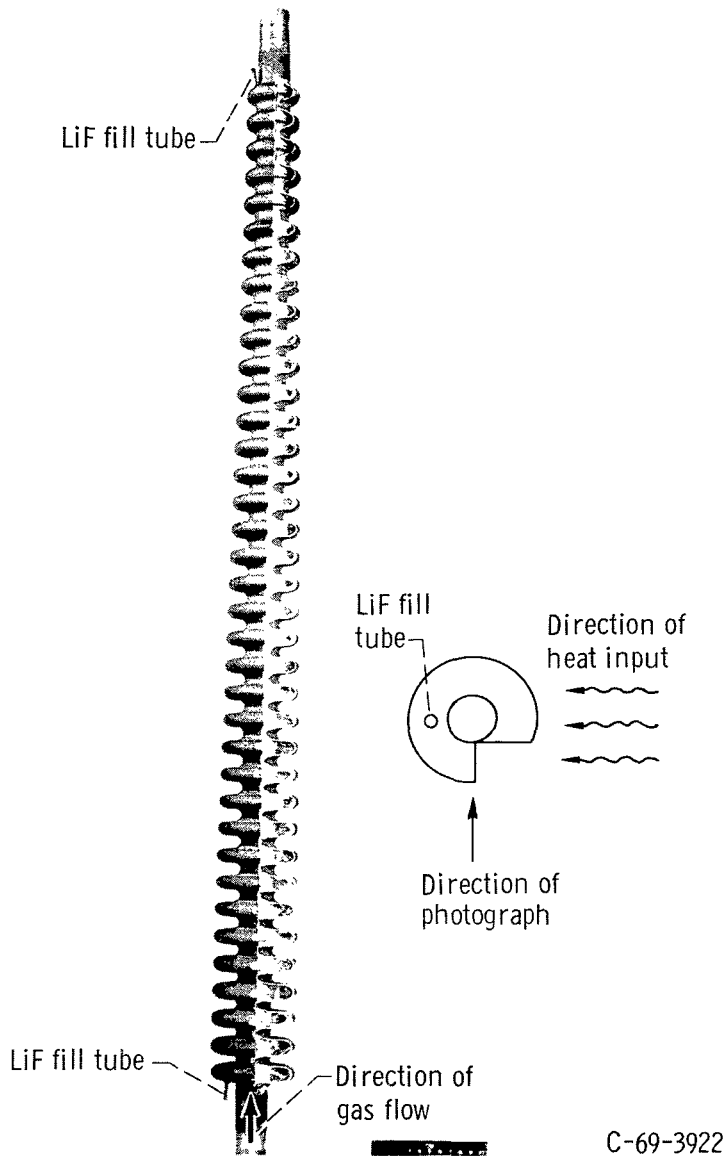

(a) Cutaway of iron titanate coated tube.

Figure 15. - Lithium fluoride (LiF) distribution on heater side.

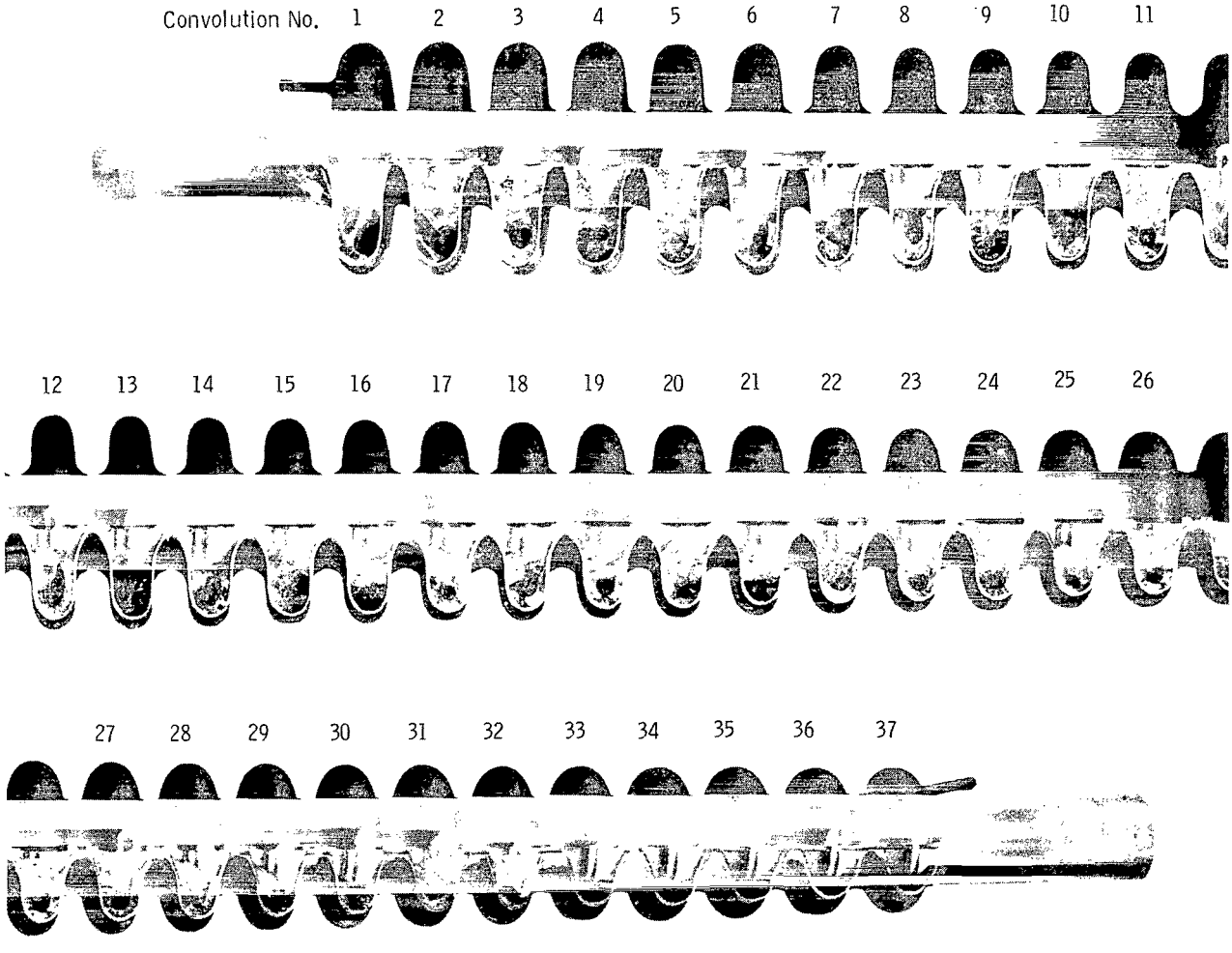

(b) Enlargement of receiver tube.

Figure 15. - Concluded.

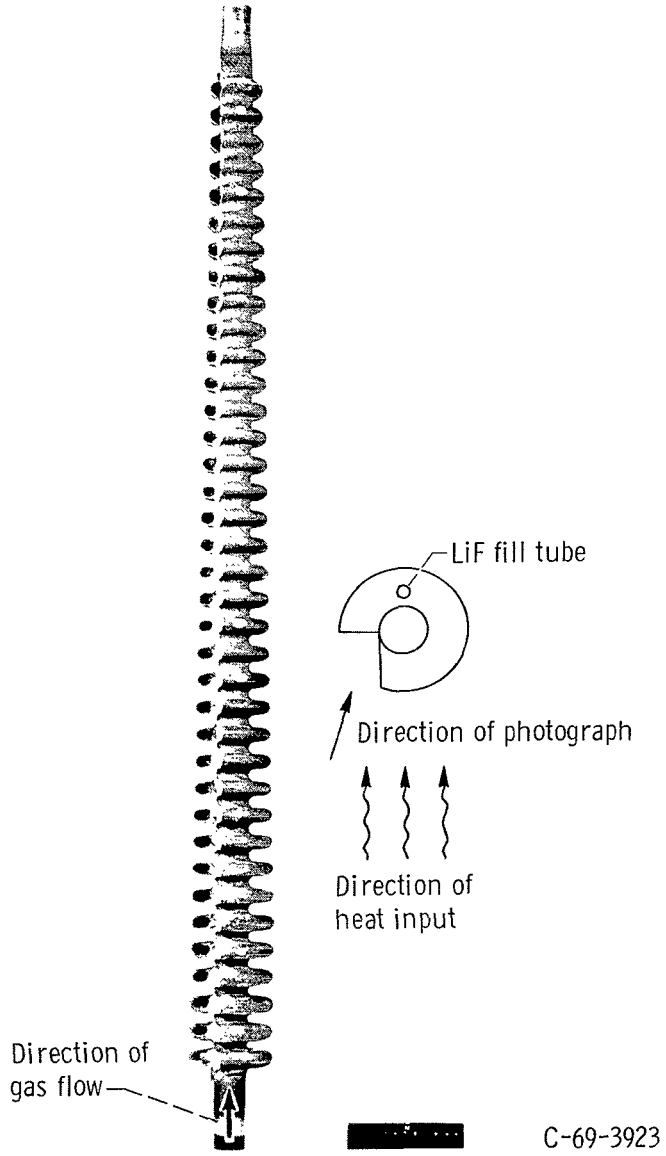

(a) Cutaway of iron titanate coated tube.

Figure 16. - Lithium fluoride (LiF) distribution on side opposite that of heater.

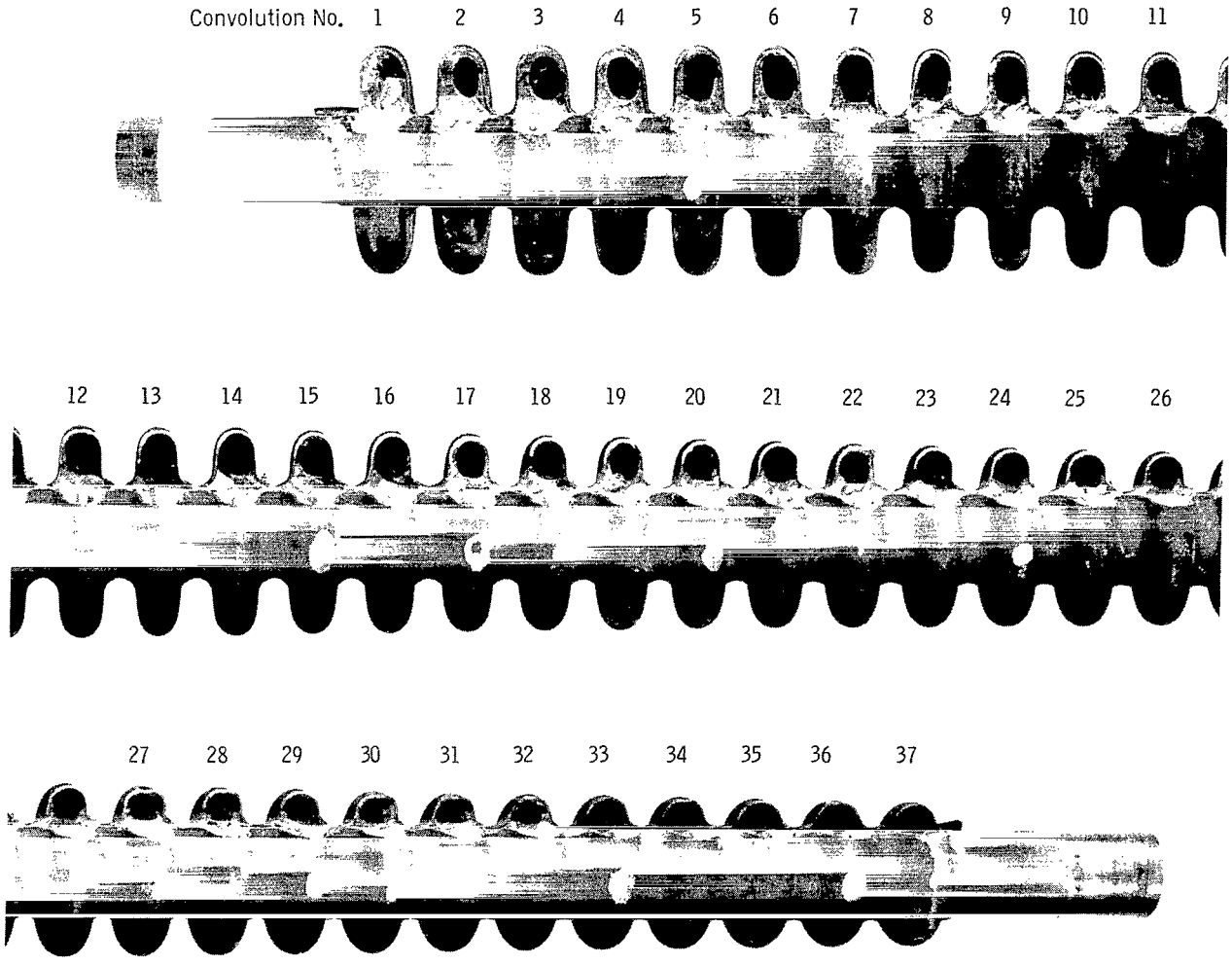

(b) Enlargement of receiver tube.

Figure 16. - Concluded.

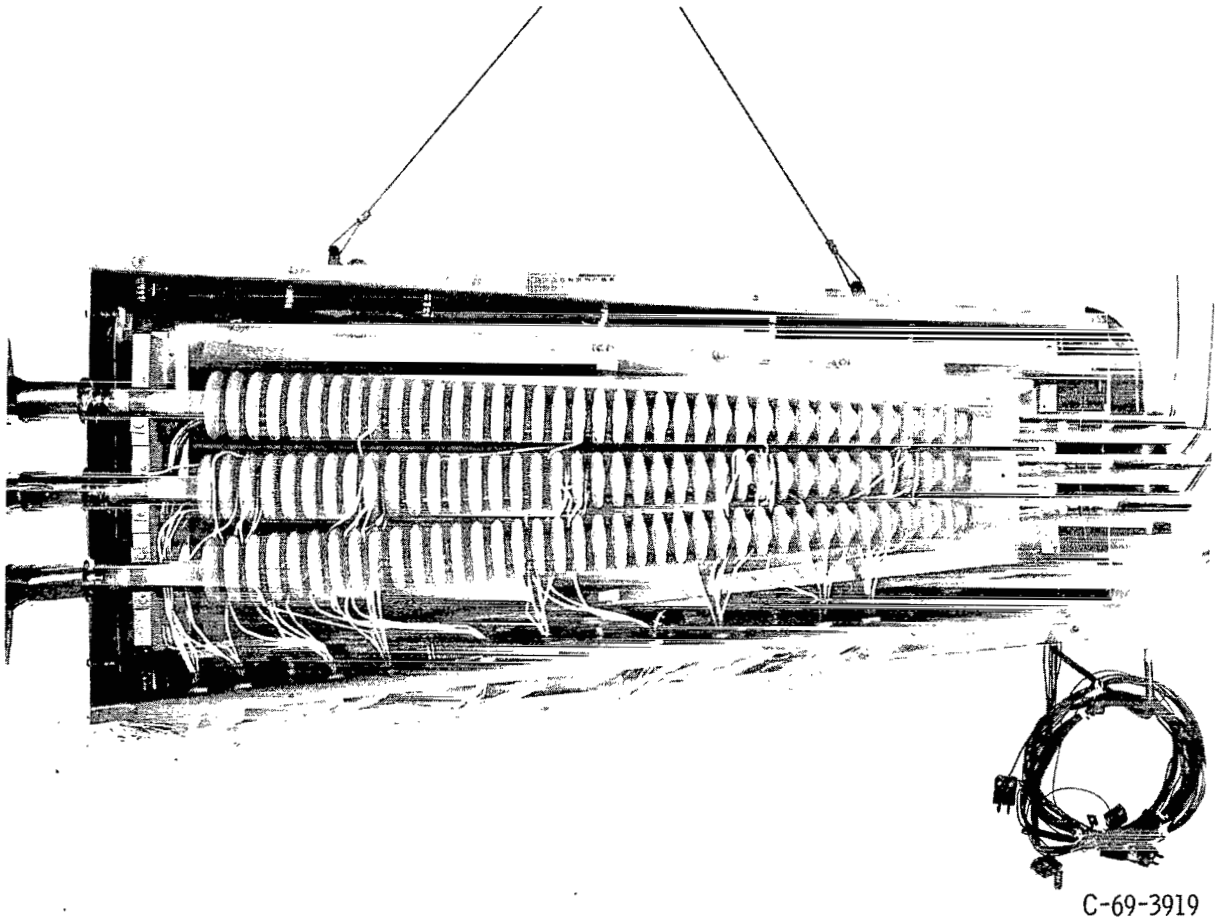

C-69-3919

Figure 17. - Grit-blasted tubes in test section after 2002-hour test.

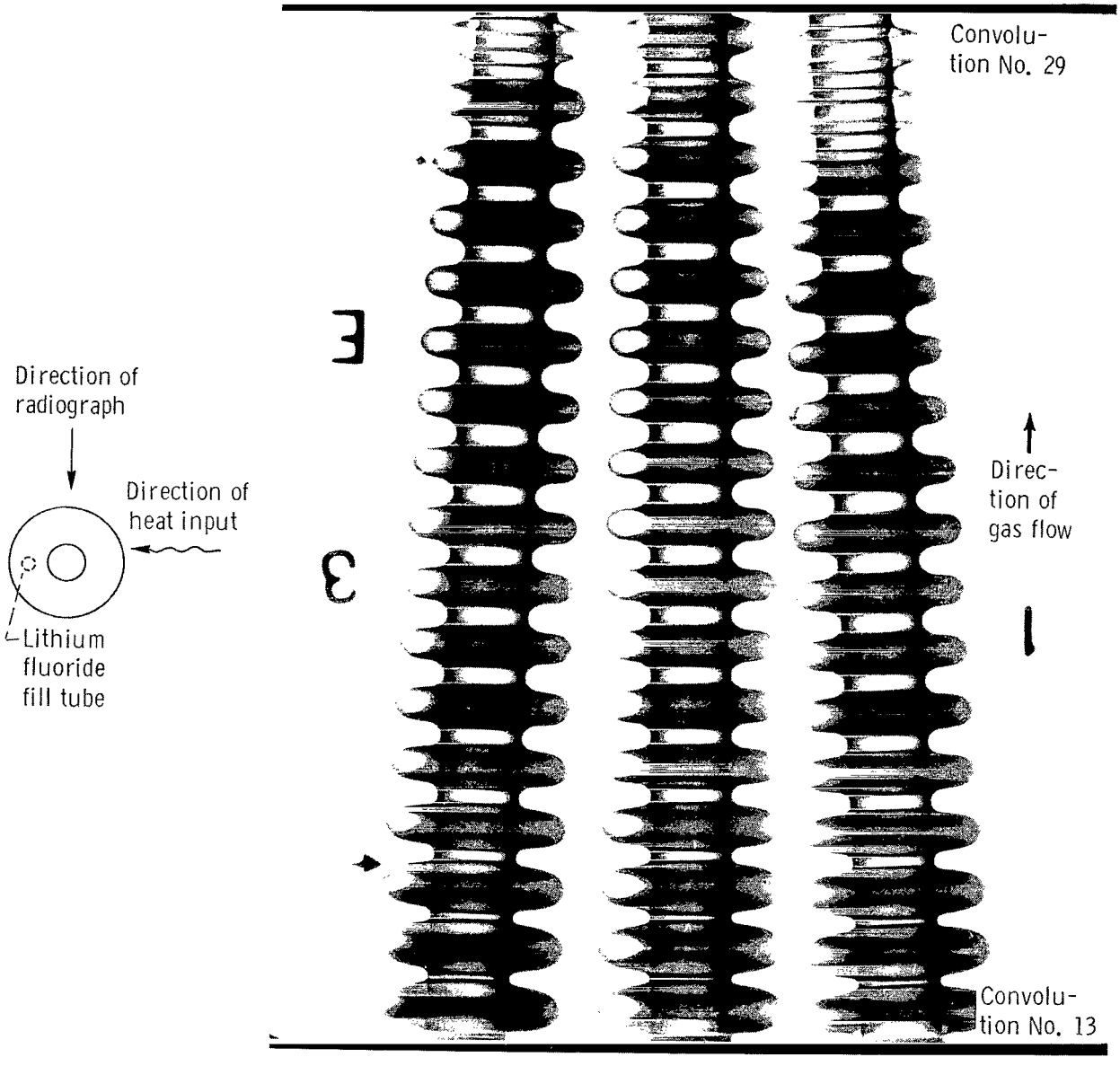

Figure 19. - Radiograph of tubes in midregion after 2002-hour test.

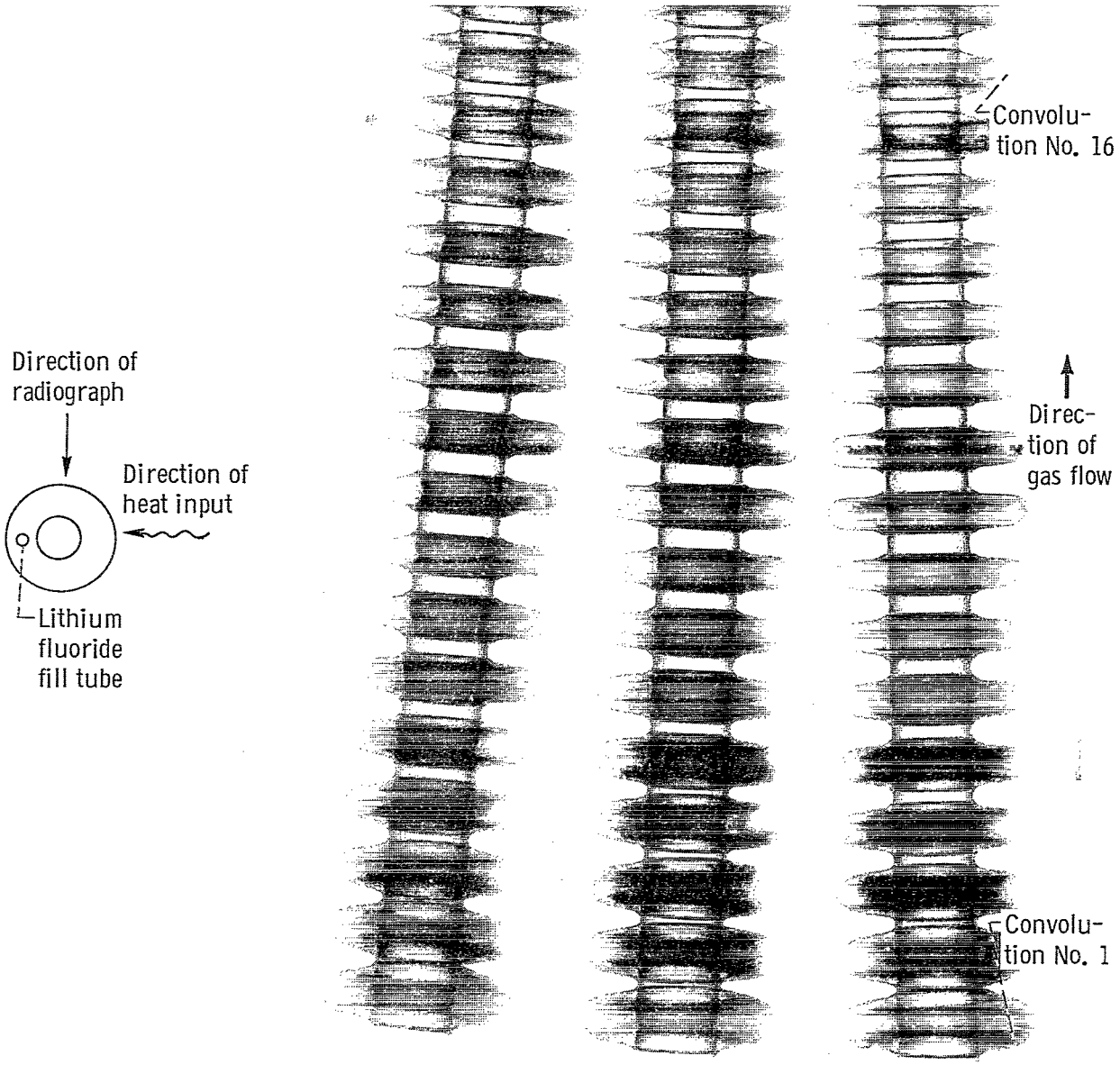

Figure 18. - Radiograph of tubes in inlet region after 2002-hour test.

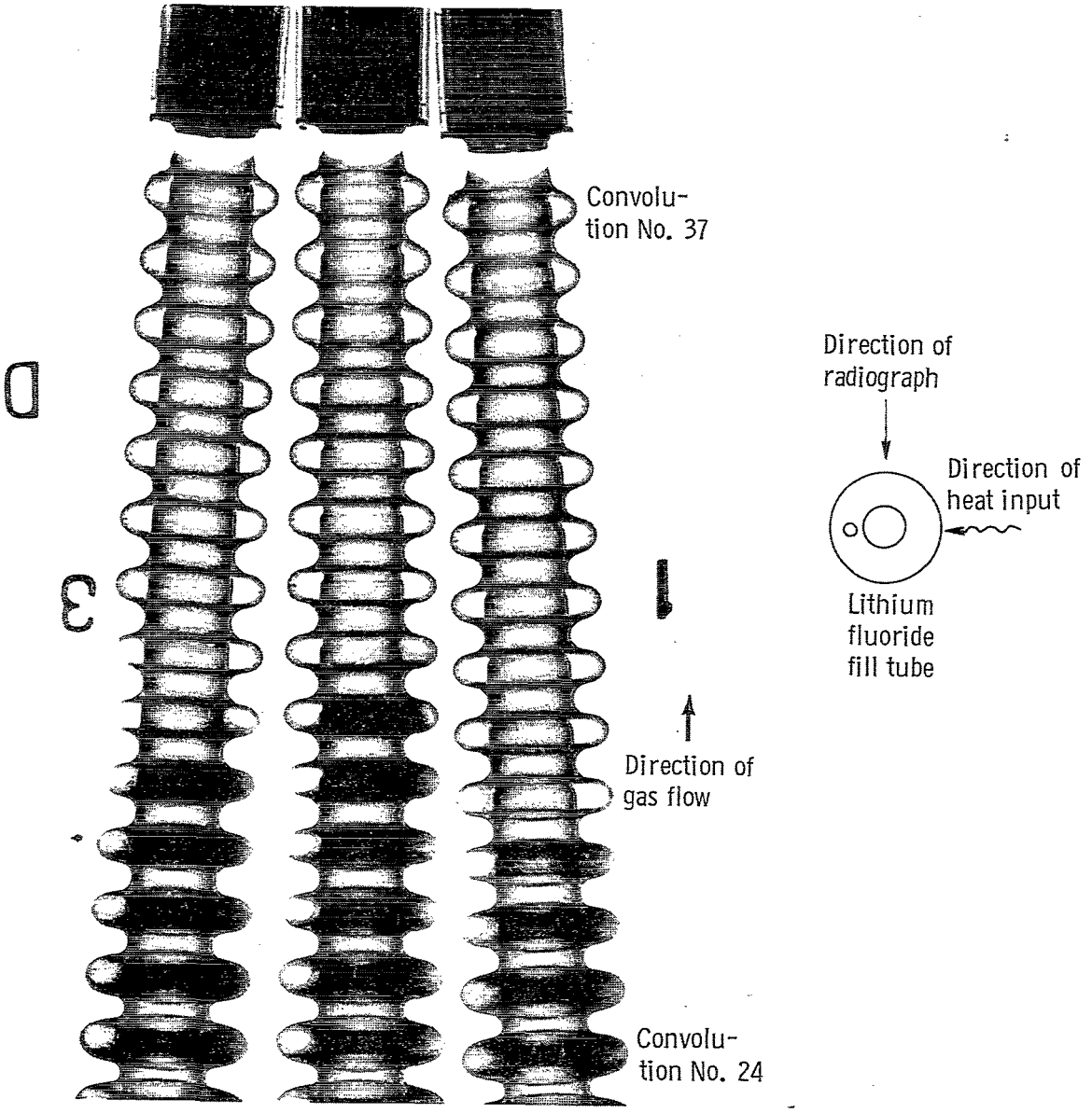

Figure 20. - Radiograph of tubes in exit region after 2002-hour test.

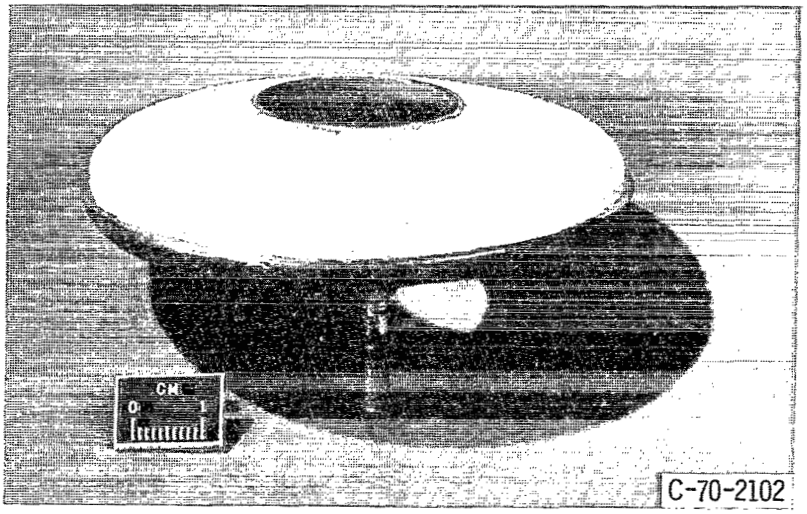

Figure 21. - Cutaway of first convolution showing fullness of LiF.

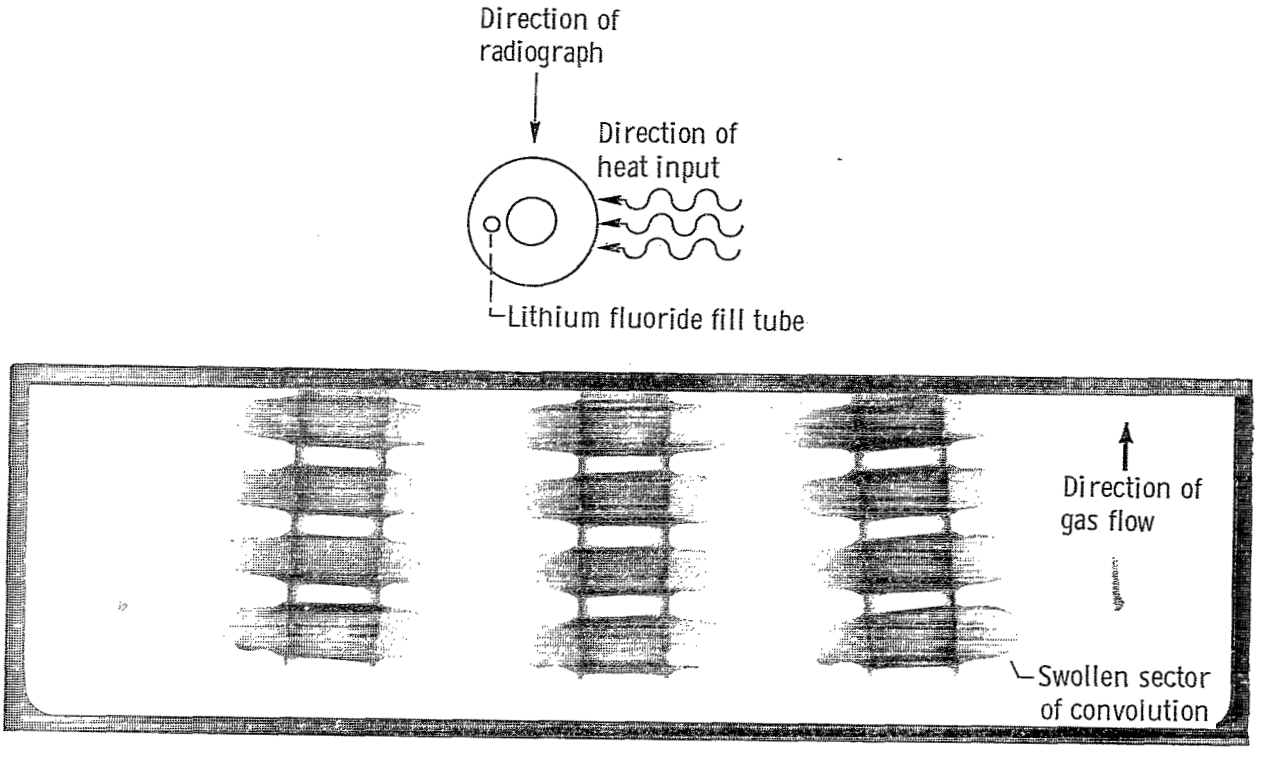

Figure 22. - Closeup radiograph of the first four convolutions from the inlet.

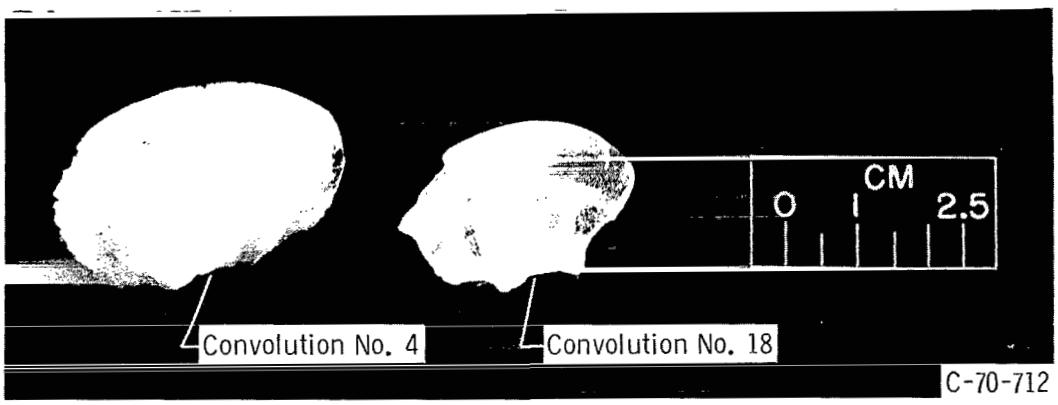

Figure 23. - Comparison of frozen lithium fluoride from convolution No. 4 and convolution No. 18.

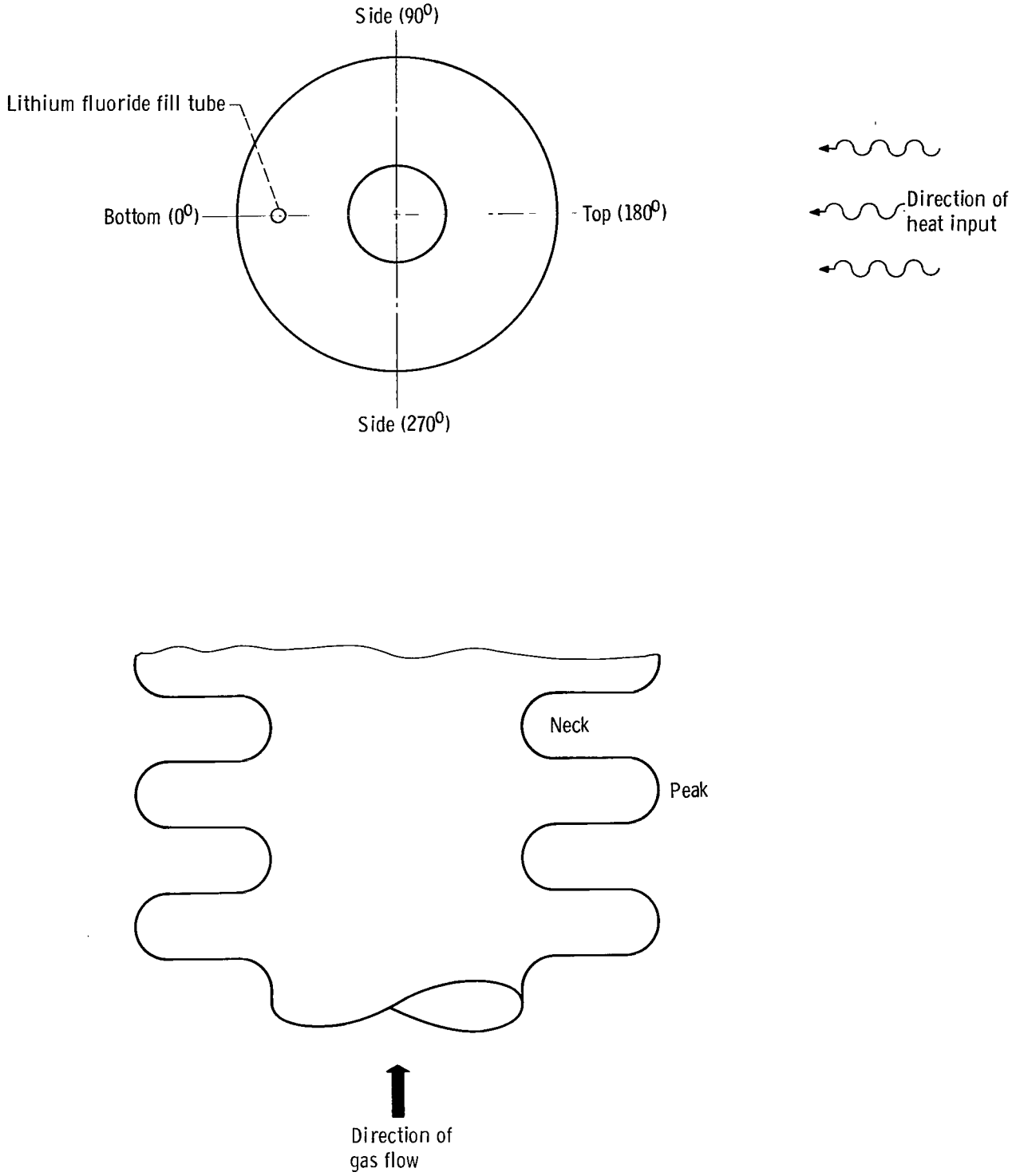

Figure 24. - Orientation of convoluted tube location to identify surface thermocouples.

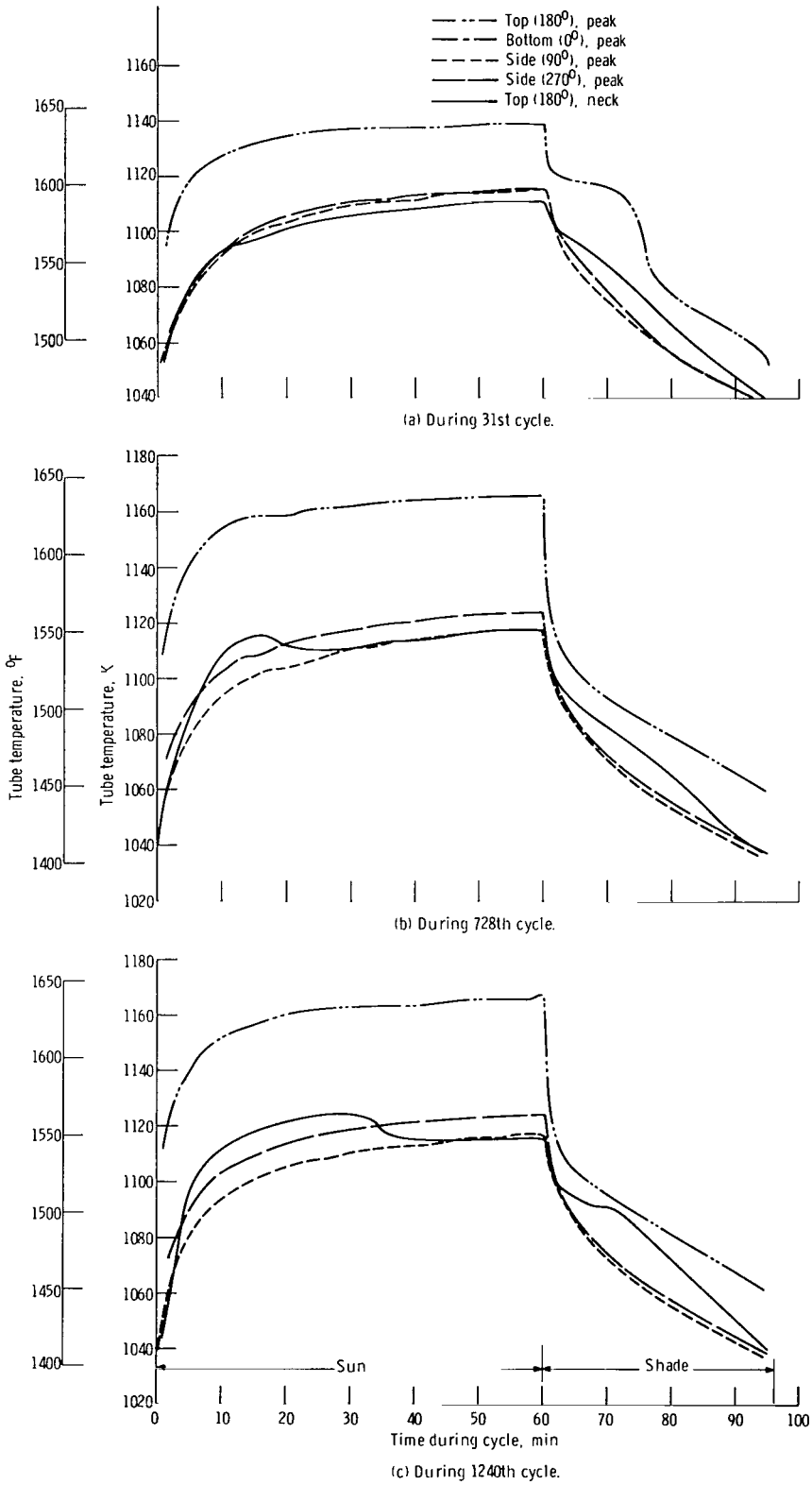

(a) During 31st cycle.

(b) During 728th cycle.

(c) During 1240th cycle.

Figure 25. - Center tube temperature distribution for convolution number 3.

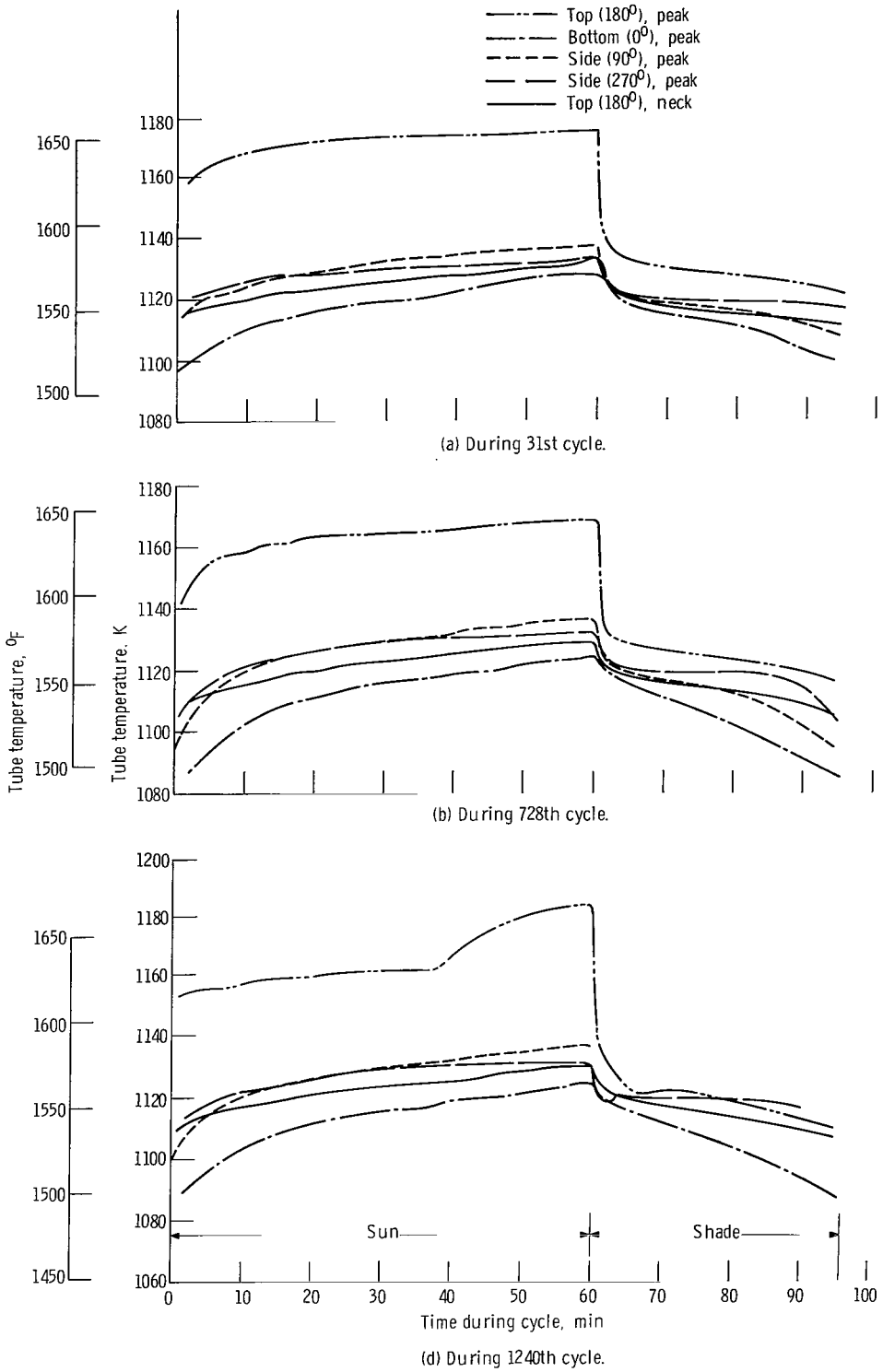

(a) During 31st cycle.

(b) During 728th cycle.

(d) During 1240th cycle.

Figure 26. - Center tube temperature distribution for convolution number 9.

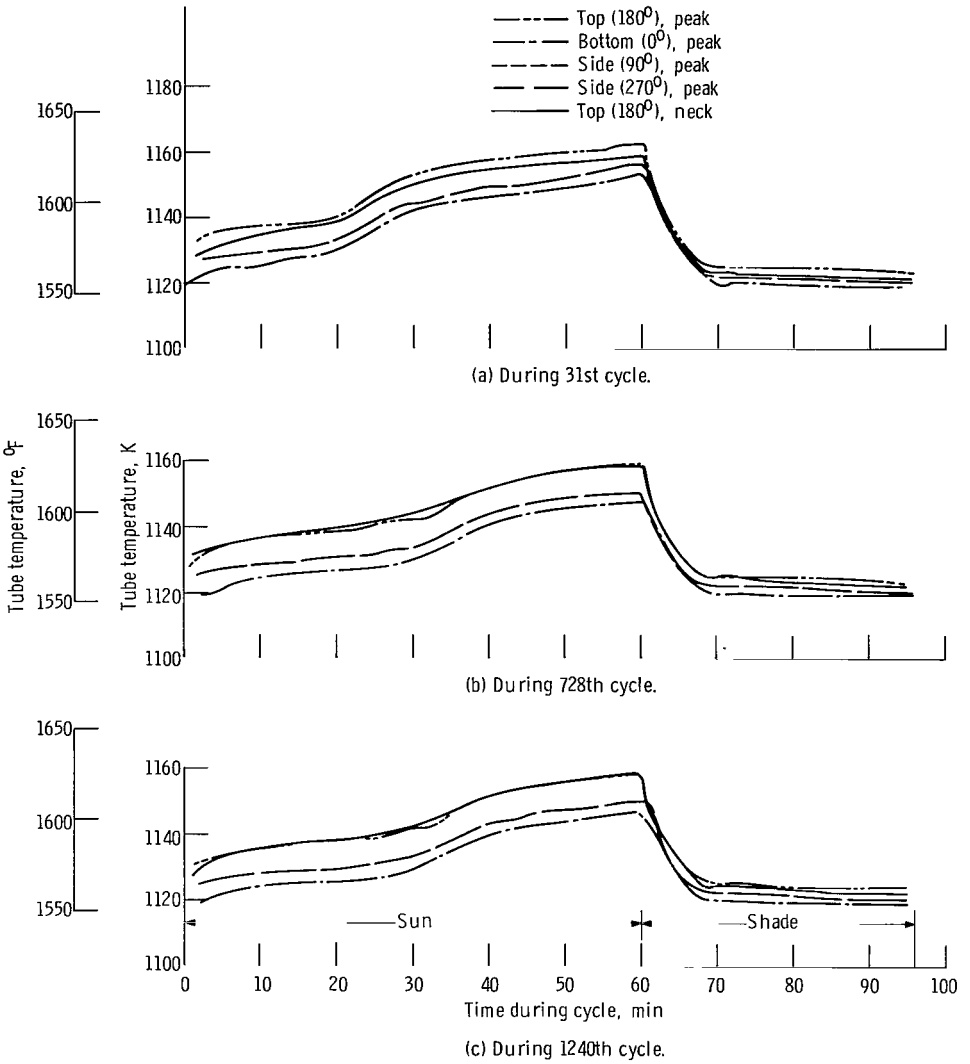

(a) During 31st cycle.

(b) During 728th cycle.

(c) During 1240th cycle.

Figure 27. - Center tube temperature distribution for convolution number 19.

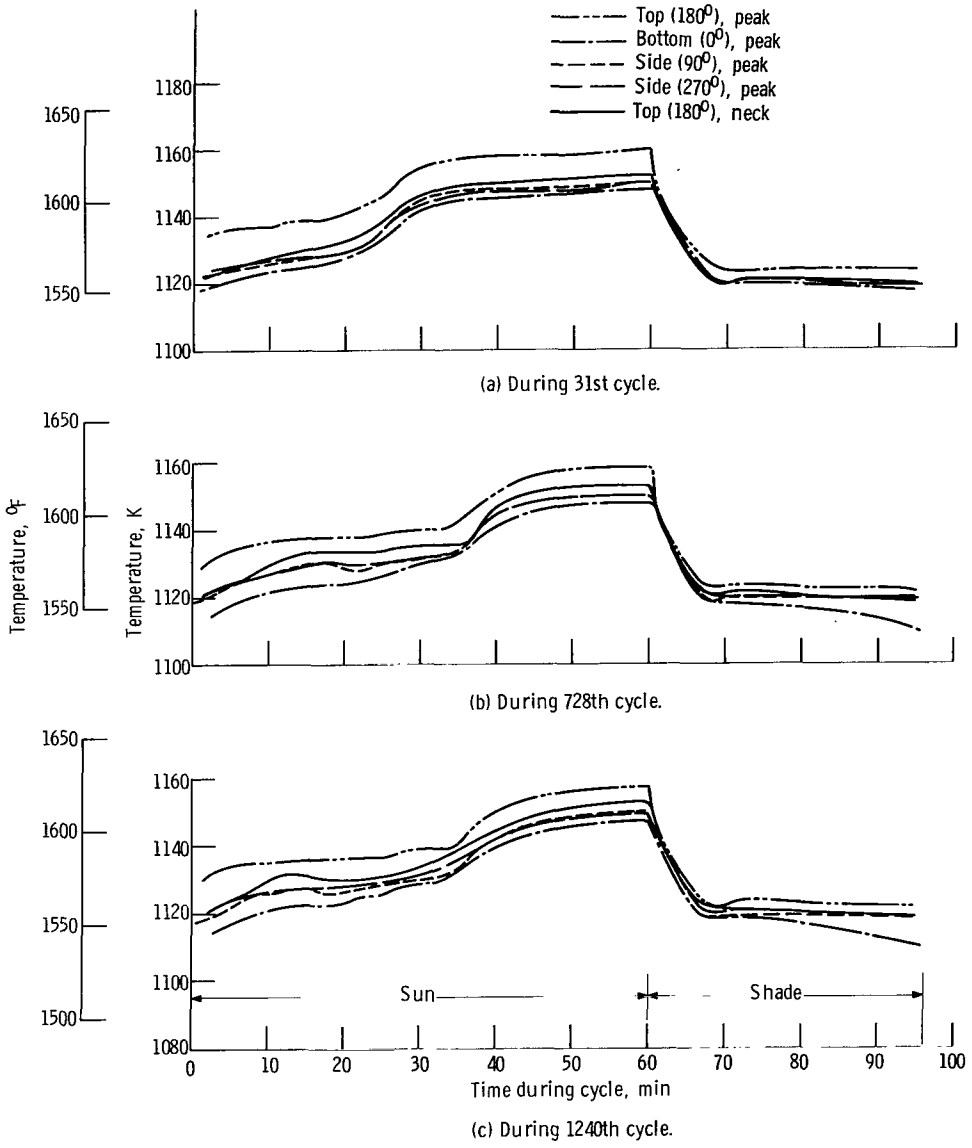

(a) During 31st cycle.

(b) During 728th cycle.

(c) During 1240th cycle.

Figure 28. - Center tube temperature distribution for convolution number 28.

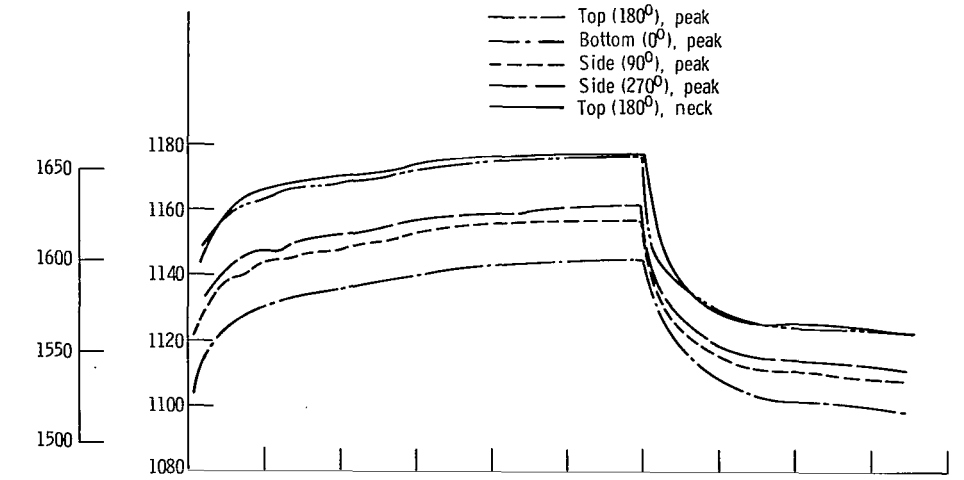

(a) During 31st cycle.

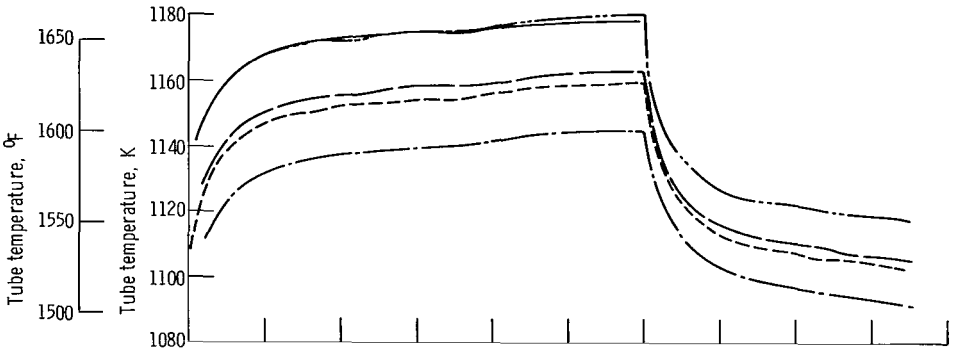

(b) During 728th cycle.

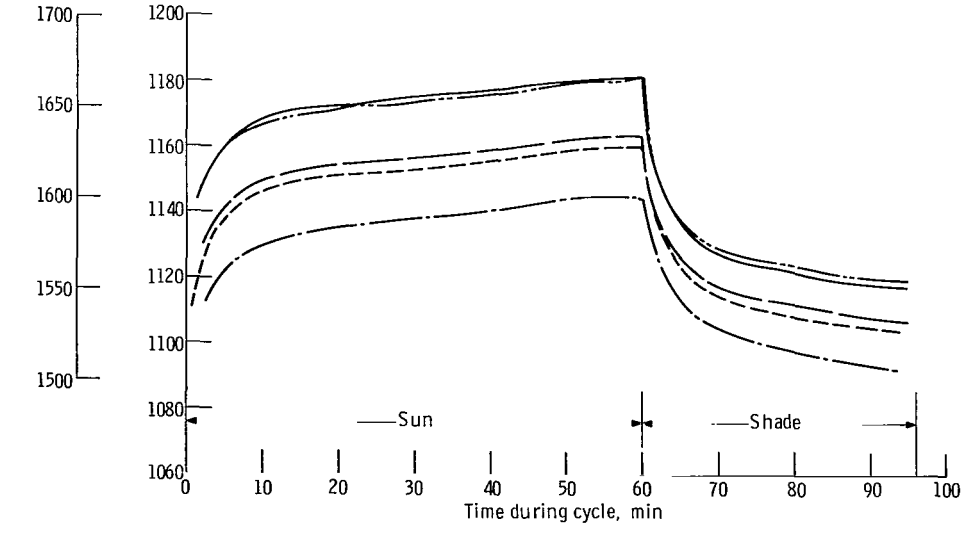

(c) During 1240th cycle.

Figure 29. - Center tube temperature distribution for convolution number 35.

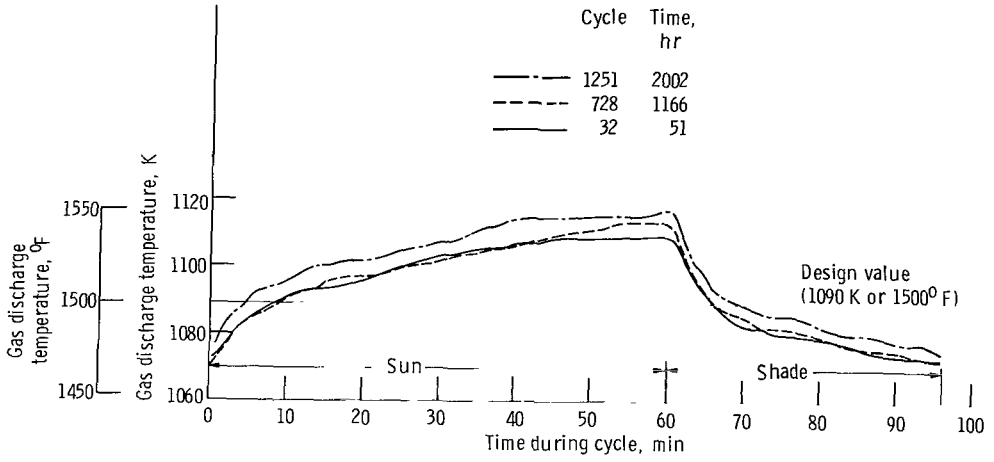

Figure 30. - Gas discharge temperature during cycles.

(a) Showing deposit on niobium reflector section - after test.

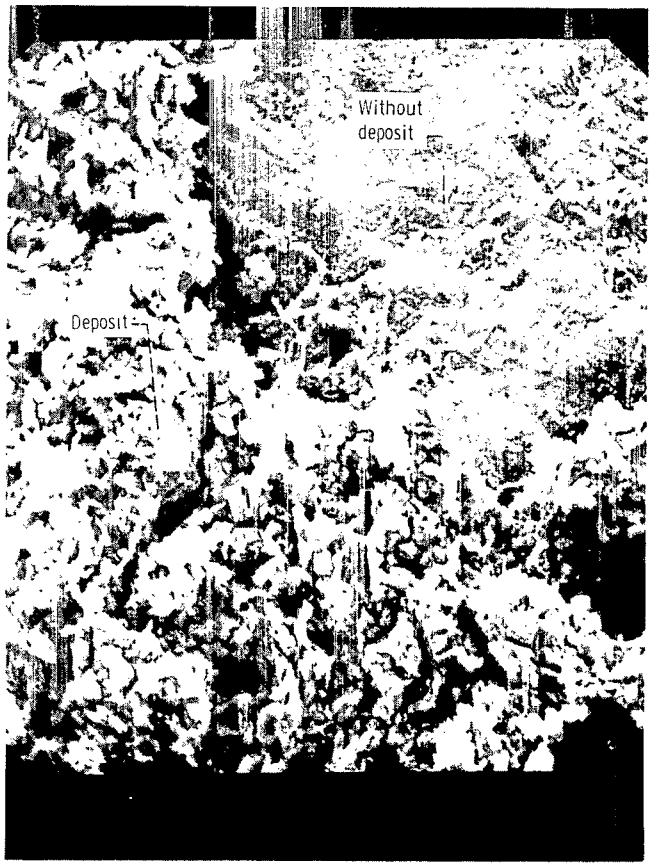

(b) Contrasting reflector section with and without deposit.

Figure 31. - Scanning electron micrographs of reflector section. X600.

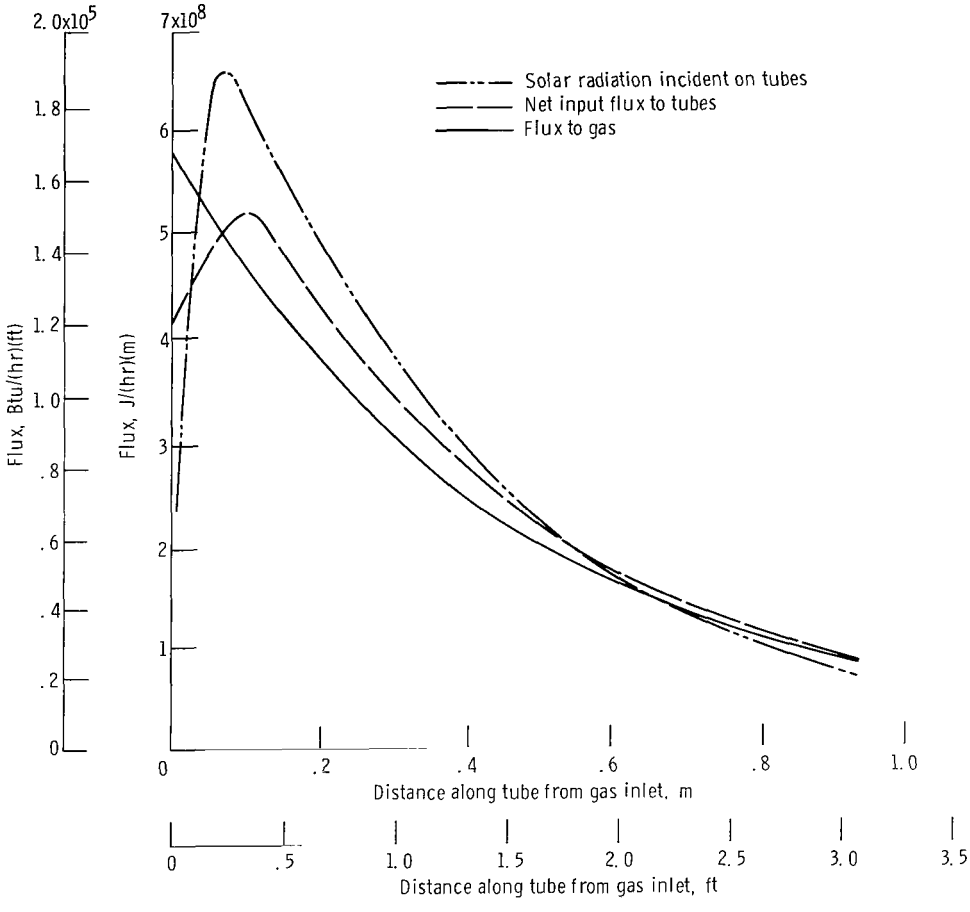

Figure 32. - Flux distributions along gas tube length.

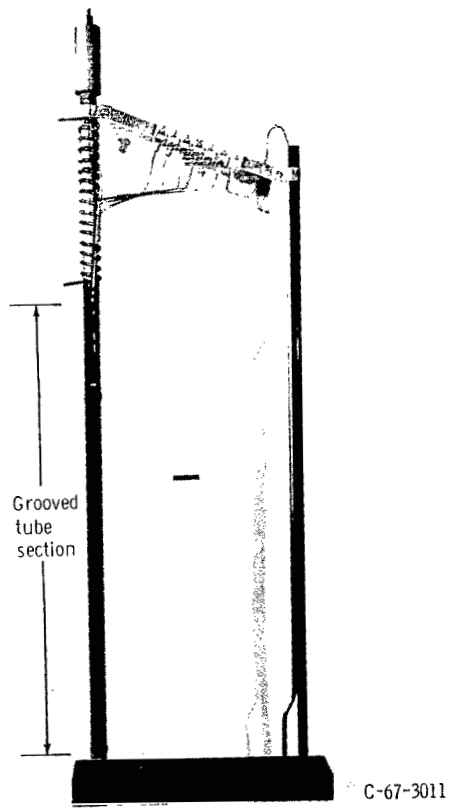

Figure 33. - Test section to determine heat-transfer performance as function of groove depth.

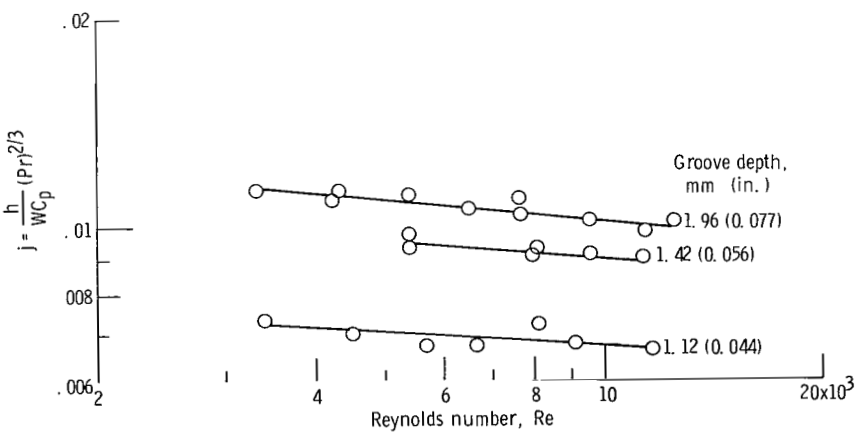

Figure 34. - Heat-transfer performance with argon as function of groove depth.

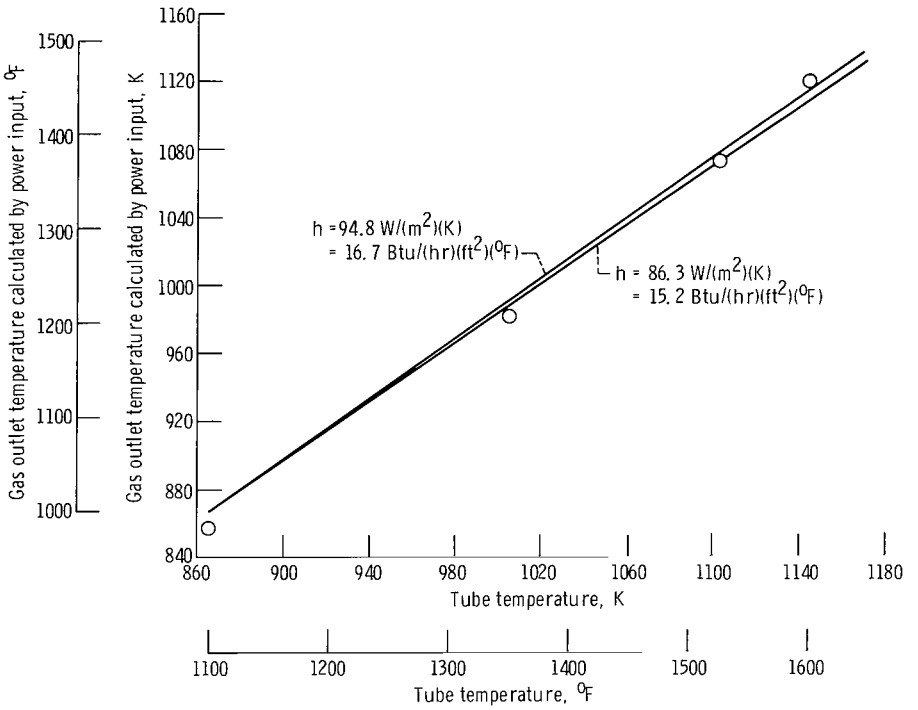

Figure 35. - Comparison of test and theoretical helium-xenon gas discharge temperature.